Student-led experimental evolution reveals novel biofilm regulatory networks underlying adaptations to multiple niches

AUTHORS

Abigail M. Matela[12], Colton W. Siatkowski[12], Changhua Yan[12], Sachin Thiagarajan[1], Vaughn S. Cooper[12]

[1]University of Pittsburgh School of Medicine, [2]Center for Evolutionary Biology and Medicine, Department of Microbiology and Molecular Genetics, Pittsburgh, PA, USA

ABSTRACT

We established a research-education partnership known as EvolvingSTEM that provides secondary school students the opportunity to conduct authentic research experiments centered on microbial evolution. These experiments are currently conducted by thousands of high school students and can offer an unprecedented window into biofilm adaptation while building a community of young researchers. Providing high school students access to research experiences improves learning and can have positive and long-lasting impacts on their attitudes towards science. Moreover, student research can make impactful scientific contributions. Through EvolvingSTEM, students evolve populations of *Pseudomonas fluorescens* in a biofilm bead model and observe heritable changes in colony morphology. Genome sequencing of 70 mutants that they picked identified parallel mutations in genes known to regulate biofilm growth (*wsp*, *yfiBNR*, *morA, fuzY*). We also uncovered novel adaptations: loss-of-function mutations in phosphodiesterase PFLU0185 that did not alter colony morphology, and mutations affecting periplasmic disulfide bond formation producing small colonies. PFLU0185 mutations consistently reached high frequencies and phenotyping revealed roles in cyclic di-GMP regulation, biofilm formation, and motility, prompting us to name this gene *bmo* (biofilm and motility optimizer). Competition experiments and microscopy demonstrated *bmo* mutants employ generalist strategies and coexist with the ancestor and specialist mutants through niche differentiation. Consequently, phenotypic diversity is maintained, with smooth (ancestral and *bmo*) colonies consistently outnumbering wrinkly and fuzzy variants. The study advances understanding of biofilm genetic architecture while demonstrating that student-led research can uncover mechanisms of microbial adaptation relevant to *Pseudomonas* infection biology and

provide transformative STEM experiences.

IMPORTANCE

Bacterial biofilms dominate microbial life, yet their evolutionary genetics remain incompletely understood. This science education project engages thousands of high school students in experimental evolution, yielding discoveries about biofilm adaptation while transforming their science education. Selected mutants included PFLU0185/*bmo*, a conserved phosphodiesterase that helps bacteria balance the competing demands of attachment and dispersal essential for biofilm life cycle success. The finding that smooth-colony generalists rather than conspicuous variants dominate biofilm adaptation adds to our understanding of the process of niche differentiation in biofilms. This work also demonstrates the power of distributed research networks for discovery of new genetic pathways of adaptation. Students gained authentic research experience, potentially inspiring them to join the next generation of scientists, while identifying mutants adapted to discrete conditions that maintain diversity within biofilms. This synergy between education and discovery offers a scalable model for addressing complex biological questions while developing scientific literacy in diverse classrooms.

INTRODUCTION

Despite being the dominant form of microbial life, our understanding of the eco-evolutionary processes occurring within biofilms is still developing. We might expect that interactions in these structured communities would be complex as cells engineer their environment by secreting polymers that bind them to a surface and protect them from stresses, competitors, or predators. Experimental evidence has shown that evolutionary dynamics within biofilms differ from those of well-mixed populations, often as a result of rapid diversification into subpopulations that inhabit new ecological niches (Stewart & Franklin, 2008; Poltak & Cooper, 2011; Traverse et al., 2013; Ellis et al., 2015; Nadell et al., 2016). Two overlapping processes can explain the origin and maintenance of high genetic diversity within biofilms. The first is environmental structure itself, which allows multiple phenotypically equivalent mutants to arise and coexist in different regions (Kassen & Rainey, 2004). The second is ecological interactions made possible by structure, for example, when an early adhering population facilitates the attachment of different types (Habets et al., 2006; Harris et al., 2021). However, the genetic and phenotypic outcomes of these processes are less clear but broadly important in natural and engineered systems, such as wastewater treatment (Røder et al., 2016) and in the clinic (Trubenová et al., 2022). For example, high-biofilm forming bacterial and fungal mutants often arise during chronic infections, are associated with increased resistance to antibiotics and immune phagocytes, and worsen patient outcomes (Hall-Stoodley et al., 2004; Flemming & Wuertz, 2019; Pestrak et al., 2018). There is a need to broadly characterize the spectrum of genotypes and phenotypes that generate biofilm diversity. Experimental evolution of microbial populations under conditions favoring biofilm combined with contemporary genomic analysis can be a powerful screen of these traits.

Our laboratory previously developed an *in vitro* model to study evolution throughout the entire biofilm life cycle of surface attachment, biofilm assembly, dispersal, and re-colonization (Poltak & Cooper, 2011). In short, bacteria are cultured in test tubes that contain growth media and a polystyrene bead, which serves as a surface for bacteria to colonize and form a biofilm. The biofilm-covered bead is then transferred to a new test tube with fresh media and a sterile bead. Beads are serially transferred to select for biofilm-adapted mutants that can disperse from the old bead and recolonize and assemble a new biofilm on the new bead every 24 hours. This model has been used by us to better understand the dynamics of biofilm evolution and

associated ecological diversification in multiple species (*Burkholderia cenocepacia*, *Acinetobacter baumannii*, *Pseudomonas aeruginosa*) under various environmental stressors (e.g., nutrients, antibiotics) (Poltak & Cooper, 2011; Traverse et al., 2013; Cooper et al., 2014; Ellis et al., 2015; O'Rourke et al., 2015; Flynn et al., 2016; Turner et al., 2018; Santos-Lopez et al., 2019; Scribner et al., 2020; Mhatre et al., 2020; Harris et al., 2021). The bead model has also been adapted by many others to address similar questions and is routinely paired with whole genome sequencing of mutant clones and evolved populations to identify causes of new phenotypes (Henriksen et al., 2022; Oakley et al., 2021; Trampari et al., 2021). A surprising finding from these studies is the extent of genetic parallelism rather than a diverse array of pathways to adaptation. Despite the intuition that the biofilm life cycle is both structured and heterogeneous, and the observation of various colony phenotypes, mutations in relatively few genes encoding major biofilm regulators accounted for most of the adaptations (Mhatre et al., 2020; Santos-Lopez et al., 2019).

One possible explanation for convergent evolution in the biofilm bead model is that each study was conducted by one or few investigators using well controlled conditions, thereby focusing selection on limited traits. Higher experimental replication by many different researchers could address this concern. For this reason and many others related to improving learning and access to authentic research, we adapted the bead model for use in secondary school classrooms (Cooper et al., 2019). In this version, students work with the harmless plant probiotic bacterium, *Pseudomonas fluorescens* strain SBW25, which is both a model of this environmentally relevant species and shares many orthologs with the opportunistic pathogen *P. aeruginosa*. This program is called EvolvingSTEM and now engages thousands of students a year in authentic microbiology research in grades 6-12 in more than 20 schools in several U.S. states. Previous research on *P. fluorescens* SBW25 identified biofilm-related adaptations to static culture conditions, where populations rapidly evolve to form a biofilm mat at the oxygen-rich, air-liquid interface (Koza et al., 2017). The evolved populations diversified into three distinct colony morphologies: (1) smooth and round (the ancestral phenotype), (2) wrinkly, and (3) fuzzy (Rainey & Travisano, 1998). It is this rapid evolution to produce pellicles that encouraged us to use *P. fluorescens* with our bead model to study its adaptation to biofilm growth with students.

113 The most conspicuous new colony phenotype seen in previous experiments is the
114 wrinkly phenotype. This phenotype commonly results from mutations in one of three genetic
115 pathways – *wsp*, *yfiBNR* (or *aws*), and *morA* (or *mws*) – that regulate the production of a
116 secondary messenger, bis-(3'-5')-cyclic dimeric guanosine monophosphate (cyclic di-GMP)
117 (McDonald et al., 2009). Cyclic di-GMP controls biofilm formation by regulating the activity of
118 several downstream genes and proteins (Jenal et al., 2017). The production of cyclic di-GMP is
119 regulated by the opposing activity of two enzyme families: diguanylate cyclases (DGCs) that
120 synthesize cyclic di-GMP and phosphodiesterases (PDEs) that degrade it (Jenal et al., 2017).
121 High cellular levels of cyclic di-GMP are associated with surface attachment and biofilm
122 production, while low levels are associated with increased motility, solitary behavior, and
123 bacterial dispersal (Laventie, Benoit-Joseph, 2020). Mutations in the *wsp*, *yfiBNR*, and *morA*
124 pathways lead to constitutive activation of a DGC, which results in overproduction of cyclic di-
125 GMP (Malone et al., 2007; McDonald et al., 2009) and, ultimately, increased biofilm formation
126 through increased production of acetylated cellulose (Spiers et al., 2002, 2003). In contrast,
127 fuzzy phenotypes are a result of mutations in *fuzY*, which encodes a β-glycosyltransferase
128 predicted to modify LPS O-antigens. Mutations in *fuzY* are thought to promote cell-cell contact
129 but the mechanistic benefit of mutations in this gene are less well understood (Ferguson et al.,
130 2013).
131
132 *P. fluorescens* populations evolved by high school students with our EvolvingSTEM
133 evolution-in-action experiment often exhibit diverse colony morphologies within and among
134 populations that resemble those seen under selection in static culture conditions (Cooper et al.,
135 2019). We wondered if the phenotypic similarities of mutants adapted to static culture and those
136 in our bead model are caused by the same underlying genetic changes, so we sequenced 70
137 clones from populations almost entirely evolved by high school students. We found that *P.*
138 *fluorescens* adapts to form biofilms on surfaces through mutations in some of the same genetic
139 pathways as those used to form pellicles in unshaken vials but also uncovered novel biofilm
140 adaptations. We then sought to identify what drives evolutionary dynamics in our bead model
141 and whether these dynamics differ when bacteria are grown in subinhibitory levels of the
142 common antimicrobial triclosan, which was used to prevent fungal and bacterial contamination
143 at some schools. This led to the discovery that biofilm adaptation in our model is primarily driven
144 by lineages that do not change colony appearance but acquire loss-of-function mutations in

145 PFLU0185, a highly conserved gene across pseudomonads encoding a DGC and dominant
146 PDE (Cai et al., 2022, 2022; Eilers et al., 2022; Eilers, Yam, et al., 2024; Wei et al., 2019).
147 Although PFLU0185 mutants share the same colony morphology as their ancestor, further
148 phenotyping revealed adaptations in biofilm formation and motility. We therefore suggest
149 renaming this locus *bmo*, for biofilm and motility regulator. Population sequencing, microscopy,
150 and multi-genotype competition experiments suggest that *bmo* mutants coexisted with their
151 ancestor and with rarer, genetically diverse lineages producing wrinkly and fuzzy colonies in
152 dynamics that can be explained by multi-niche selection (Brisson, 2018).
153
154 **RESULTS**
155
156 **Student-led experiments rapidly uncover diverse phenotypes**
157 Our EvolvingSTEM evolution-in-action experiment allows students to observe bacterial
158 populations evolving and diversifying within days as they adapt to a daily selection regime to
159 complete the entire biofilm life cycle of dispersal, surface attachment, and biofilm maturation.
160 Students work with a harmless plant probiotic bacterium, *P. fluorescens* strain SBW25. As the
161 populations evolve, students can observe at least two types of phenotypic change. First, as high
162 biofilm-forming mutants increase in frequency in the population, students often see a more
163 robust layer of biofilm form in their test tubes at the air-liquid interface. Second, students can
164 observe changes in the colony morphologies of bacteria grown on agar plates. While the
165 ancestral population produces only smooth, circular colonies, evolved populations often exhibit
166 diverse, conspicuous colony morphologies within and among populations (Fig. 1).
167
168 Students from three high schools – Winnacunnet High School (WHS, Hampton, NH,
169 N=~250), Pittsburgh Science and Technology Academy (Pittsburgh, PA, N=25), and Allderdice
170 High School (Pittsburgh, PA, N=24) – conducted experiments under slightly different conditions.
171 Changes to the experimental protocol were made to accommodate class requirements and
172 increase the accessibility of EvolvingSTEM in varied classroom settings (our updated protocol
173 can be found in supplemental materials). While WHS used standard aseptic technique, in other
174 schools, we added the commonly used antimicrobial compound triclosan to the media and agar
175 plates to broadly inhibit bacterial and fungal contamination. *Pseudomonas* species are known to
176 tolerate or resist triclosan (Schweizer, 2001; McFarland et al., 2021), and this eliminates the

177 need to use a flame in schools that do not have access to Bunsen burners and/or do not feel
178 comfortable having students work near an open flame. Another difference was that WHS
179 aerated growing bacterial cultures on a roller drum, which was not available in most classrooms,
180 so we switched to using orbital shakers to aerate growing cultures.
181
182 Students plated samples of their bead-attached bacterial populations on agar at the
183 beginning and end of the experiment. Ancestral *P. fluorescens* clones produce only smooth,
184 round colonies, and this was the only morphology identified on the early plating day. Most bead-
185 adapted populations contained wrinkly colony variants on the final plating day, and some had
186 fuzzy and small colony variants (Fig. 1). Wrinkly and fuzzy colony variants had a similar
187 appearance to those identified when *P. fluorescens* is under selection for the formation of
188 biofilm mats in static culture conditions (Koza et al., 2017). While our experimental design also
189 selects for biofilm-adapted mutants, it differs from static selection experiments in that bacteria
190 must colonize a new surface each day, completing the entire biofilm life cycle of dispersal,
191 attachment, biofilm assembly, and matrix building. We therefore explored if the convergent
192 colony phenotypes we identified in these experiments was the result of convergent mutational
193 targets by sequencing the genomes of wrinkly and fuzzy clones from independent populations.
194 In addition, we sequenced the genomes of smooth colonies, which were identical in appearance
195 to the ancestor, and small colony variants, which were the only other unique morphology noted
196 in these experiments (Fig. 1).
197
198 **Biofilm adaptations include mutations affecting cyclic di-GMP production, LPS O-antigen**
199 **structure, and periplasmic protein folding**
200 Two remarkable properties of this collection of mutant genomes deserve highlighting
201 before we explore the genes affected or their functional implications. First, in 55 of 70 mutants,
202 only one mutation was identified, meaning that this single mutation experienced strong selection
203 to rise to a detectable frequency and, in most cases, change the colony morphology (Table 1,
204 Table S1). Consequently, the biofilm bead model serves as a potent forward genetic screen for
205 single mutations that influence biofilm-related fitness. Of the remaining 15 mutants, 13 had two
206 mutations and one had three mutations. Second, the extent of site-specific parallelism in these
207 mutants is extraordinary: 13 individual mutations occurred more than once in apparently
208 independent clones. One SNP in *wspF* was observed in six clones and another 33bp deletion in

209 *yfiR* was observed five separate times. This observation suggests extremely strong selection for
210 certain mutations, a locally higher mutation rate, or both. Overall, 23 unique genes became
211 mutated and were affected by a roughly equal mix of small insertion/deletions (indels) and SNPs
212 with fewer larger deletions. This spectrum of mutations demonstrates that *P. fluorescens*
213 experiences strong selection for a narrow set of traits in the biofilm bead model that often favors
214 identical mutations in independent experiments.
215
216 The genomes of 57 clones with wrinkly phenotypes were sequenced from 50
217 independently evolved biofilm populations. In agreement with previous studies on biofilm
218 formation in static culture conditions, causative mutations were identified in the *wsp*, *yfiBNR*,
219 and *morA* pathways (Fig. 2, Table 1), which supports a critical role for these pathways in biofilm
220 regulation under diverse selective regimes. Mutations in the *wsp* pathway were the most
221 common cause of wrinkly phenotypes across all sequenced clones, with approximately 70%
222 having a single causative mutation in this pathway. Mutations were primarily found in *wspF*
223 (PFLU1224, 33 clones), followed by *wspA* (PFLU1219, 6 clones). In addition, a single clone had
224 a 335 base-pair deletion that overlapped the coding regions of *wspC* (PFLU1221) and *wspD*
225 (PFLU1222), resulting in a WspC-WspD fusion protein. The *yfiBNR* pathway was the second
226 most common cause of wrinkly phenotypes, with approximately 16% of clones having a single
227 causative mutation in *yfiR* (PFLU5211, 9 clones). Mutations in *morA* (PFLU5329, 5 clones) were
228 the least common cause of wrinkly phenotypes, with approximately 9% of clones having a single
229 causative mutation. Surprisingly, all three clones isolated at Allderdice had mutations in two
230 pathways. These clones contained a single, nonsynonymous SNP in the PDE domain of *morA*.
231 One clone had an additional nonsense mutation in *wspF*; one had an additional missense
232 mutation in *wspA*; and one had an additional deletion in the linker region between the DGC and
233 PDE domains of *morA*. These mutants indicate that the sequential acquisition of multiple
234 mutations in pathways influencing cyclic-di-GMP metabolism can be beneficial.
235
236 Fuzzy mutants were identified in evolved populations at several schools, although less
237 frequently than wrinkly mutants. While we did not sequence any fuzzy mutants from high school
238 experiments, two fuzzy mutants isolated in the laboratory had predicted loss-of-function
239 mutations in *fuzY* (PFLU0478) (Fig. 3). In addition, we sequenced the genomes of five small
240 colony variants isolated by students and in the laboratory. These mutants contained single

241 mutations in a predicted two-component system sensor histidine kinase, *dsbS* (PFLU4380), or
242 in the operon it is predicted to regulate, *dsbD* (PFLU4382)-*dsbG* (PFLU4384) (Fig. 3). Three
243 clones had an in-frame deletion in the N-terminal region of *dsbS*, one clone had a 110 base-pair
244 deletion that overlapped the coding regions of *dsbE* (PFLU4383) and *dsbG*, resulting in a DsbE-
245 DsbG fusion protein, and one clone had a mutation in the intergenic region upstream of *dsbR*
246 (PFLU4381) and *dsbD* (Fig. 3). Lastly, we also sequenced clones from five evolved populations
247 that retained the ancestral smooth morphology. Although one smooth clone had no mutations,
248 four clones had a mutation in a gene encoding both DGC and PDE domains, PFLU0185, and
249 this was the only mutation identified in three clones (Fig. 3). We have named this gene *bmo* for
250 its roles in biofilm formation and motility, which are further described below.
251
252 **Strong selection for mutations in *bmo* during adaptation to the experimental biofilm life**
253 **cycle**
254 We were intrigued by the discovery of mutations in a DGC-PDE encoding gene that did
255 not change the mutant colony phenotype. Although an objective of the EvolvingSTEM program
256 is to visually demonstrate adaptation by natural selection by observing novel colony phenotypes
257 after selection for improved biofilm formation, in fact, most populations have a majority of
258 colonies that retain the smooth appearance of the ancestor after one week of passage. This
259 suggests that focusing only on colony variants may miss biofilm adaptations. To address this
260 limitation, we conducted a 15-day evolution experiment in which we used whole-population,
261 whole-genome sequencing to identify all mutations reaching appreciable frequency in biofilm
262 populations regardless of whether they alter colony appearance. We also replicated this
263 comparison in media containing triclosan, which we use in classrooms to guard against
264 contamination and which appears to accelerate rates of diversification. Specifically, four
265 replicate biofilm populations were propagated with and without 25μg/mL triclosan for 15 days.
266 We plated the bead-attached portion of each population after 4, 8, 11, and 14 transfers to
267 observe phenotypic changes to population colony morphologies over time and performed
268 whole-population, whole-genome sequencing after 2 and 14 transfers (Table S2, Fig. 4). We
269 noted three distinct colony morphologies, wrinkly, fuzzy, and small, in addition to the ancestral,
270 smooth phenotype. Populations grown in triclosan had moderately increased diversity on the
271 earliest plating day, but this diversity decreased over the course of the experiment, with all
272 populations having over 95% smooth colonies by the final plating. Populations that were grown

273 without triclosan maintained slightly higher diversity over time, and all populations had between
274 90-95% smooth colonies by the final plating (Fig. 4).
275
276 Surprisingly, mutations in the *bmo* locus were the only gene-level parallel genetic
277 change in all biofilm populations, and they rose to detectable frequencies by the third day of the
278 experiment in media containing triclosan, but not in media without triclosan (Fig. 4, Table S2).
279 Multiple independent mutations in *bmo* were present within each of the three biofilm populations
280 with added triclosan at day 3 at 16.7%, 42.3%, and 50% cumulative frequency, and by day 15
281 all eight biofilm-adapted populations had *bmo* mutants at >16% cumulative frequency. The only
282 other notable biofilm-related mutation that we observed was in *fuzY*, which reached a frequency
283 of 11.2% in one population that was grown without triclosan. Furthermore, three of the four
284 populations grown with added triclosan gained mutations in a transcription factor, *anr*
285 (PFLU4570), and one of the genes it regulates, *hemN* (PFLU4568). These mutations may be
286 adaptations to growth in triclosan and will be the subject of future study.
287
288 **Mutants are differentiated in biofilm phenotypes including attachment, assembly, and**
289 **motility**
290 We predicted that mutations in *bmo* achieved the highest frequencies and repeatedly
291 evolved in our biofilm selection model because they are best adapted to the cyclical
292 requirements to attach to the plastic bead, assemble biofilms, and then disperse to colonize a
293 new bead. We therefore characterized the motility, biofilm production, and cyclic di-GMP
294 production for a representative *bmo* loss-of-function mutant with a single nucleotide insertion
295 that results in a premature stop codon truncating both the DGC and PDE domains (Table 1). We
296 compared its biofilm associated phenotypes to a representative wrinkly (*wspF* Q185*) and fuzzy
297 (*fuzY* Q11*) mutant, along with the *P. fluorescens* SBW25 ancestor from which these mutants
298 evolved.
299
300 We first compared three common types of bacterial motility – swarming, swimming, and
301 twitching. All biofilm-adapted mutants had reduced swarming and swimming motility in
302 comparison to the ancestor (Fig. 5A, 5B). *wspF* mutants were the least motile, while *fuzY* and
303 *bmo* mutants had intermediate phenotypes. Twitching motility was not displayed by any biofilm-

304 adapted mutants or the ancestor, confirmed by comparison to *Pseudomonas aeruginosa* PAO1
305 which possesses twitching motility (Fig. S1).
306
307 To estimate biofilm production by each mutant, we adapted the traditional crystal violet
308 96-well plate assay (O'Toole & Kolter, 1998) to better align with how bacteria form biofilms in
309 our bead model. Bacteria were cultured for 24 hours in test tubes containing media and two
310 plastic beads. We quantified total biofilm production by staining one bead with crystal violet,
311 removing excess stain by washing the bead in water, and solubilizing biofilm-bound crystal
312 violet by vortexing the bead in solvent. We quantified biofilm population size by vortexing and
313 dilution-plating from the second bead. When grown in QB medium, *bmo* and *wspF* mutants
314 have the highest total biofilm production and population size (Fig. 5C, 5D). One caveat to note is
315 that *wspF* mutant populations often acquire compensatory, suppressor mutations that can rise
316 to high frequencies in overnight cultures, so between 20%-40% of the colonies counted had a
317 smooth, ancestral phenotype. When grown in media with added triclosan, total biofilm
318 production is doubled in *bmo*, *fuzY*, and the ancestor and quadrupled in *wspF* (Fig. 5C, 5D).
319 Moreover, the population size of all genotypes is less than half that observed in triclosan-free
320 media (Fig. 5C, 5D). Planktonic growth is also slower when triclosan is included in the media
321 and final population sizes are smaller (Fig. S2).
322
323 To determine how these biofilm-adapted mutations affect cyclic di-GMP metabolism, we
324 used a GFP reporter plasmid that responds to the intracellular concentration of cyclic di-GMP to
325 estimate these changes. Levels of cyclic di-GMP differed significantly among *P. fluorescens*
326 mutants following 24 hours of growth in QB media (Fig. 5E). Cyclic di-GMP concentrations were
327 highest for *bmo* and *wspF* mutants, with *wspF* producing nearly double the amount of cyclic di-
328 GMP as *bmo*. Surprisingly, the *fuzY* mutant produced approximately half as much cyclic di-GMP
329 as the ancestor, although this gene is not reported to have a role in the regulation of cyclic di-
330 GMP. Taken together, these results demonstrate that *bmo* regulates biofilm formation and
331 motility and loss-of-function mutations in this gene allow for the optimization of biofilm
332 production and planktonic growth in our bead model.
333
334 We sought to understand how the different macroscopic and regulatory phenotypes of *P.*
335 *fluorescens* mutants generated distinct microscopic biofilm phenotypes. We therefore used

336 confocal microscopy to image biofilms produced by our representative *bmo*, *wspF*, and *fuzY*
337 mutants as well as the ancestor that contained a constitutively active fluorescent reporter
338 inserted at a neutral site on the chromosome. Both the ancestor and *bmo* formed relatively
339 confluent biofilms of even thickness and their similar appearances suggest that they would
340 compete for the same niche space on the bead (Fig. 6). In contrast, the *fuzY* biofilm was more
341 clumped and uneven in thickness and coverage, whereas the *wspF* biofilm was surprisingly
342 sparse, with small, dense clusters (Fig. 6). It is notable that we imaged biofilms on glass slides
343 rather than on the polystyrene beads on which these mutants evolved, and that the supernatant
344 of the *wspF* cultures contained large aggregates that did not adhere well to glass. To explore
345 how these mutants interact in a diverse biofilm, we imaged mutants with different fluorescent
346 markers that were co-cocultured in pairs (Fig. S3). Overall, the observed patterns of biofilm
347 assembly agreed with predictions from mutant growth alone, with interspersed and confluent
348 growth by *bmo* and the ancestor but fewer discrete patches of different sizes and forms
349 produced by *wspF* and *fuzY.* Taken together, these images indicate that biofilm mutants in
350 different pathways are ecologically distinct and produce clusters or coatings of varying biomass
351 and form, both alone and in mixture.
352
353 **Genetic diversity during biofilm selection is maintained by competition and niche**
354 **differentiation**
355 An important and unusual finding from these studies is that *P. fluorescens* populations
356 grown in the biofilm bead model rapidly and repeatedly diversify into multiple phenotypes and
357 genotypes that coexist, with no genotype ever reaching 100%. This observation implies that
358 selection acts strongly on mutants that inhabit different niches of varied capacity. This leads to
359 the prediction that if putative niche specialists are mixed in equal amounts and propagated, their
360 frequencies should equilibrate according to the capacity of each niche and the relative
361 competitiveness of each mutant in conditions of niche overlap (e.g., growth on a common
362 carbon source). We created a mixed population of the three, representative biofilm-adapted
363 mutants *bmo*, *wspF*, and *fuzY* and their *lac*-marked ancestor. We used this mixed population to
364 inoculate six replicate cultures grown in our bead model of biofilm growth for four days without
365 triclosan and plated daily to determine the frequency of each genotype on newly colonized
366 beads (Fig. 7). As predicted, all genotypes coexisted within each population, with *wspF* and
367 *fuzY* mutants generally at low frequencies and the *bmo* mutant and ancestor at intermediate

368 frequencies. In addition, frequencies of *bmo* and WT were anticorrelated in half of the replicates,
369 which suggests they occupy differentiated but overlapping niches, as the microscopy indicated
370 and ecological literature supports (Fig. 6) (Caplat et al., 2008; Chesson, 2000). We used linear
371 regression to test this hypothesis for all genotype combinations and found a significant, negative
372 relationship for the *bmo* mutant frequency with frequencies of all other genotypes, which is
373 consistent with competition (Table 2, Fig. S4). In summary, our model of the biofilm life cycle
374 exerts strong, parallel selection for different phenotypes that balance biofilm production, growth,
375 dispersal, and reattachment in different ways. Mutants adapted to different aspects of these
376 traits can coexist by invading in conditions in which they are more fit, while declining in
377 conditions where they are less competitive.
378
379 **DISCUSSION**
380
381 **Student experiments discover new genetic pathways of adaptation to the biofilm life**
382 **cycle**
383 Involving secondary school students in distributed scientific experiments in their own
384 science classrooms offers complementary promises, including: 1) a high level of replication that
385 can broadly test a common hypothesis, and 2) developing a community of teachers and
386 learners who are connected by a common set of research skills, experiences and findings.
387 Here, we not only report evidence that both promises can be met, but also that students
388 contributed to expanding our knowledge of the genetics of adaptation to the biofilm life cycle.
389 Their experiments with the biofilm bead model selected for phenotypes that excel during daily
390 cycles of dispersal, recolonization, and biofilm assembly. By picking many representative clones
391 with these phenotypes and then genotyping them by whole-genome sequencing, we use
392 experimental evolution as a powerful forward genetic screen. This approach identified mutants
393 that support previous findings from pellicle selection experiments and also uncovered novel
394 adaptive pathways within the biofilm lifestyle. These findings support the hypothesis that biofilm
395 selection acts on traits governed by a few central regulators, leading to strong parallel evolution
396 across experiments. They also reveal that different selective environments, for example
397 associated with varied implementation in classrooms, can uncover alternative adaptations in
398 novel pathways to biofilm formation. Because most of these mutants contain only one mutation
399 in their genome, the relationships between genotype and phenotype are direct. In this section,

400 we discuss predicted molecular and biochemical effects of these mutants in detail, several of
401 which strengthen or modify existing models of *Pseudomonas* biofilm gene regulation. We begin
402 by analyzing mutations producing the well-known wrinkly and fuzzy colony morphologies and
403 follow with discussion of the potential causes of beneficial small colony variants.
404
405 **Student-selected colony variants support previous findings of genetic pathways**
406 **important for biofilm formation**
407 The most common cause of wrinkly phenotypes was mutations in the *wsp* pathway, a
408 chemotaxis-like system composed of 7 genes: *wspA-R*, under the control of a single promoter
409 (Fig. 2) (Bantinaki et al., 2007). WspA is a methyl-accepting chemotaxis protein that is anchored
410 at the cytoplasmic membrane by the scaffolding proteins WspB and WspD. Upon sensing an
411 environmental signal, conformational changes in the WspA-B-D complex result in WspA being
412 methylated by WspC, a constitutively active methyltransferase. This begins a signaling cascade
413 that activates WspE, a histidine kinase response regulator. WspE goes on to activate WspR, a
414 DGC, through phosphorylation, increasing levels of cyclic di-GMP and ultimately leading to
415 increased biofilm formation through increased cellulose production (Spiers et al., 2002, 2003).
416 WspE also phosphorylates WspF, a methylesterase that negatively regulates the system by
417 demethylating WspA. In general, the Wsp pathway mutations we identified are predicted to
418 cause constitutive production of cyclic di-GMP and, consequently, increased biofilm formation.
419 We identified deletions in *wspA* that have been shown *in P. aeruginosa* to lock the pathway on
420 in a methylation-independent manner (A. Xu et al., 2021), whereas nonsynonymous mutations
421 in the *wspA* signaling domain likely disrupt the stability of its trimer-of-dimer interactions,
422 increasing WspE activation (O'Connor et al., 2012; Kessler et al., 2021). The mutation
423 producing a WspC-WspD fusion protein likely leads to hypermethylation of WspA because it
424 physically links WspC to the WspA-B-D complex (Kessler & Kim, 2022). The many different
425 mutations in *wspF* include nonsynonymous substitutions, insertions, and deletions, including
426 frameshift and nonsense mutations that led to the introduction of premature stop codons (Fig.
427 2). These mutations almost certainly interfere with WspF activation and/or its ability to
428 demethylate WspA (O'Neal et al., 2022; A. Xu et al., 2021).
429
430 The second most common cause of wrinkly phenotypes were mutations in the *yfiBNR*
431 pathway, which is composed of three genes under the control of a single promoter (Fig. 2). YfiN

432 is a DGC that is localized to the cytoplasmic membrane and negatively regulated by the
433 attachment of the periplasmic YfiR protein (Malone et al., 2010, 2012). In response to
434 membrane stress, YfiB, a lipoprotein located at the outer membrane (Malone et al., 2012),
435 adopts an elongated conformation, which allows it to bind to and sequester YfiR (Li et al., 2018;
436 M. Xu et al., 2016). YfiN is therefore released from its negative regulation and able to catalyze
437 cyclic di-GMP production, promoting biofilm formation (Fig. 2). The C-terminal region of *P.*
438 *aeruginosa* YfiR is predicted to contain the attachment site to YfiN (Malone et al., 2012; Yang et
439 al., 2015); therefore, the *yfiR* missense and nonsense mutations we discovered in this region
440 may eliminate YfiR's ability to bind to YfiN. *P. aeruginosa* YfiR forms a dimer in its active form
441 via salt bridges formed by R98 and D80 and hydrogen bonds between T76 (Yang et al., 2015).
442 Notably, five *yfiR* mutants experienced a 33bp deletion from T75 to T85 in *P. fluorescens* that
443 removes these homologous regions involved in dimerization. In addition, both this deleted
444 region and the downstream 33bp deletion contain or are located close to conserved cysteine
445 residues that in *P. aeruginosa* form disulfide bonds important for proper protein folding (Yang et
446 al., 2015). Deletions in these regions are therefore likely to lead to protein misfolding that
447 inhibits YfiR's ability to bind YfiN, thereby derepressing the DGC which promotes a biofilm
448 lifestyle.
449
450 Mutations in *morA* were the third most likely cause of wrinkly phenotypes. MorA is a
451 single protein localized to the cytoplasmic membrane that contains two PAS sensor domains as
452 well as active DGC and PDE domains, so it can catalyze both production and degradation of
453 cyclic di-GMP (Fig. 2) (McDonald et al., 2009; Phippen et al., 2014). We identified two identical
454 nonsynonymous substitutions in the DGC, three mutations affecting the linker region between
455 DGC and PDE domains that likely cause conformational changes that increase DGC activity
456 (Mhatre et al., 2020), and three identical mutations in the PDE that appear to disrupt its activity
457 (Fig. 2). The elevated biofilm of all these mutants indicates that their effects increase cyclic di-
458 GMP levels.
459
460 Fuzzy colony phenotypes are caused by loss-of-function mutations in *fuzY* (Fig. 3). In *P.*
461 *fluorescens* SBW25, *fuzY* is part of a 5 gene operon that was predicted to encode a β-
462 glycosyltransferase that plays a role in modifying lipopolysaccharides (LPS) O-antigens, the
463 outermost portion of the LPS (Ferguson et al., 2013). The reciprocal best match of *fuzY*

464 homologs in *P. aeruginosa* strain PAO1 is *wapH*, which participates in synthesis of the LPS core
465 (Lam et al., 2011). In either case, in addition to roles in pathogenesis and symbiosis, O-antigen
466 structure plays an important role in bacterial adhesion and cohesion (Lerouge & Vanderleyden,
467 2002). In *P. aeruginosa*, O-antigen mutants exhibit increased cell-cell cohesion and increased
468 adhesion to glass surfaces (Lau et al., 2009). In our bead selection experiment, we expect that
469 mutations in *fuzY* are beneficial because they increase both cell-cell and cell-surface contact,
470 which would provide an advantage in adhering to the surface of the bead.
471
472 **Student findings uncover new pathways to biofilm adaptation predicted to disrupt**
473 **periplasmic protein folding**
474 Biofilm evolution experiments with our bead model often select for small colony variants
475 with increased Congo Red binding, which is consistent with higher cellulose production (Fig. 1;
476 Fig. S5). These phenotypes were consistently caused by mutations in a pathway that regulates
477 the formation of disulfide bonds, *dsbRS* and *dsbDEG*, which is critical for some proteins to be
478 properly folded into their active state conformation (Fig. 3). Most knowledge of enzymes
479 involved in the formation of disulfide bonds comes from studies in *Escherichia coli* (J. C. A.
480 Bardwell et al., 1991; J. C. Bardwell et al., 1993). In *E. coli*, the periplasmic oxidoreductase
481 DsbA catalyzes formation of disulfide bonds but is thought to perform this reaction
482 indiscriminately by introducing bonds between neighboring cysteines (Bader et al., 2000; J. C.
483 A. Bardwell et al., 1991). Proteins that require disulfide bond formation between nonconsecutive
484 cysteines undergo further processing through the activity of disulfide isomerases (DsbC and
485 DsbG) that rearrange these bonds (Berkmen et al., 2005; Hiniker & Bardwell, 2004; Manta et
486 al., 2019).
487
488 In *P. aeruginosa*, homologs of the regulatory two-component system *dsbRS* have been
489 shown to regulate the activation of *dsbDEG* homologs partly by binding copper ions (Yu et al.,
490 2022). Based on this study, we predict that evolved *dsbS* mutants lead to altered
491 phosphorylation of *dsbR* which interferes with its regulation of *dsbDEG*. The evolved intergenic
492 mutation is found in the predicted DsbR binding site and would therefore reduce *dsbDEG*
493 transcription. The evolved DsbE-DsbG fusion mutant likely interferes with the ability of these
494 proteins to fold properly, with the downstream consequence of misfolded periplasmic proteins.
495 Taken together, we predict that all mutations in this pathway result in misfolded periplasmic

496 proteins, although the exact proteins that are affected are unknown. Interestingly, in *P.*
497 *aeruginosa*, deletion of *dsbA* led to a small colony variant phenotype that was hypothesized to
498 be a result of YfiR misfolding due to its cysteine residues that contribute to dimerization,
499 resulting in constitutive activation of YfiN and elevated cyclic-di-GMP (Malone et al., 2012).
500 However, the small colonies produced by *dsb* mutations differ from the wrinkly mutants of
501 caused by *yfiR* mutations, suggesting different effects on biofilm requiring further study.
502
503 **Discovery of frequent mutations in phosphodiesterase *bmo* that do not change colony**
504 **morphology**
505 Clones retaining the ancestral, smooth colony phenotype at the end of evolution
506 experiments often acquired a mutation in *bmo*, a gene with both DGC and PDE domains that is
507 highly conserved in the genus *Pseudomonas* and predicted to function primarily as a PDE (Fig.
508 3) (Eilers, Hoong Yam, et al., 2024; Wei et al., 2019). A representative mutant showed
509 intermediate levels of both biofilm production and motility, leading us to name this gene *bmo* for
510 its role in balancing both biofilm and motility. We predict that our model selects for *bmo* mutants
511 because they act as biofilm generalists that have improved attachment and biofilm formation
512 compared to their ancestor, while also maintaining the ability to disperse from the old bead to
513 recolonize the new bead. Characterization of multiple biofilm-associated phenotypes supports
514 this hypothesis. Compared to the ancestor and the hyper-biofilm *wspF* mutant, *bmo* has
515 intermediate motility, cyclic di-GMP, and overall biofilm attachment phenotypes, whereas its
516 cellular attachment to the bead is as high as *wspF* (Fig. 5). Moreover, *bmo* biofilm phenotypes
517 are nearly identical to the LPS mutant *fuzY*, although *bmo* has somewhat improved motility,
518 attachment, and overall biofilm formation, along with significantly greater cyclic di-GMP levels. It
519 is also notable that *bmo* mutants appear to be selected more frequently in media containing
520 triclosan, suggesting the stress imposed by this compound interacts with the *bmo* regulatory
521 pathway that remains to be defined.
522
523 *P. aeruginosa bmo* homologs have been shown to influence biofilm formation and
524 regulate basal levels of cyclic di-GMP. A deletion mutant of the *P. aeruginosa* PA14 homolog
525 (PA14_03720) had reduced swimming motility and increased twitching motility in comparison to
526 wild-type PA14 (Ha et al., 2014). Deletion mutants of the *P. aeruginosa* PAO1 homolog
527 (PA0285, *pipA*) have increased biofilm formation, aggregation, Psl production, and cyclic di-

528 GMP production, and decreased swimming motility (Cai et al., 2022; Eilers et al., 2022; Wei et
529 al., 2019). A recent study that compared deletion mutants of *bmo* homologs in *P. aeruginosa*
530 strains PA01, PAK, and PA14, and *P. putida* strain KT2440 found that these mutants had
531 increased early attachment (at 4, 6, and 8 hours) in comparison to their wild-type counterparts
532 and that the magnitude of these differences depended on strain background (Eilers, Hoong
533 Yam, et al., 2024). Among the 22 unique mutants detected by deep sequencing populations
534 evolved in the bead biofilm model, most are predicted to (1) cause loss-of-function by
535 introducing premature stop codons or (2) negatively affect PDE function or PAS domain
536 signaling through nonsynonymous SNPs (Sup. Table 1). We predict these mutants resemble
537 the representative mutant clone we studied (Fig. 5) by having a higher basal level of cyclic di-
538 GMP that improves their attachment to the bead surface and biofilm formation.
539
540 **Phenotypic differentiation among mutants reflects niche differentiation that enables**
541 **coexistence**
542 The spectrum of biofilm phenotypes arising in these experiments suggests that they
543 exploit different ecological conditions, which could explain both their rapid emergence and
544 subsequent coexistence. This model was well supported by confocal microscopy of biofilms
545 produced by individual mutants and mixed pairs (Fig. 6, Fig. S3) but these measurements were
546 on glass rather than polystyrene and did not allow mutants to reach equilibrium frequencies.
547 Therefore, we mixed representative mutants of each morphology and tracked their frequencies
548 over a week of passage. The *bmo* mutant and the ancestor appeared to compete as their
549 intermediate frequencies oscillated, whereas *wspF* and *fuzY* mutants rapidly declined but were
550 maintained at low (~5-10%) frequencies (Fig. 7). The cycling between the *bmo* mutant and the
551 ancestor can be explained by their occupying overlapping but distinct niches (Brisson, 2018;
552 Chesson, 2000), whereas the persistence of *wspF* and *fuzY* at lower frequencies suggests they
553 inhabit more differentiated biofilm niches but are outcompeted by the other genotypes under
554 most conditions (Fig. 6, Fig. S3, Table 2). These dynamics agreed with the phenotypic
555 dynamics from the 15-day evolution experiment (Figure 4), in which biofilm-adapted mutants
556 with distinct wrinkly and fuzzy colony morphologies rapidly arose and persisted at low
557 frequencies while ancestral colony morphologies consistent with persistence of the ancestor
558 and biofilm-adapted *bmo* mutants predominated. These overall interactions conform to a model
559 known as multi-niche selection (Levins, 1963), which requires that each species has a selective

560 advantage in some habitats while others are superior in other habitats, with areas of niche
561 overlap. We suggest that the repeated emergence and maintenance of genotypes with
562 differentiated niches within the biofilm life cycle provides a clear example of how variable
563 environments can favor balanced polymorphisms (Martin et al., 2016; Poltak & Cooper, 2011).
564 Given the ubiquity of microbial biofilms undergoing regular cycles of attachment, aggregation,
565 dispersal, and reattachment, we can expect genetic and phenotypic heterogeneity like that
566 shown here to be widespread. This diversity may therefore be expected in biofilms produced by
567 natural populations of *P. fluorescens* in and around plants or in those produced by its relative *P.*
568 *aeruginosa* in the built environment or when establishing opportunistic infections.
569

570 **Building a community of learners studying biofilm evolution who understand its**
571 **biomedical relevance**

572 We began the EvolvingSTEM project in 2013 with the aim of teaching evolution and
573 genetics in high school classrooms through an authentic bacterial evolution experiment. Our
574 rationale was that the predominant way of teaching natural selection through passive, historical
575 examples of speciation would be less effective than the experience of seeing evolution in action
576 in student-led experiments. We showed that high school students achieved greater learning of
577 content meeting Next Generation Science Standards (States, 2013) in a prior study (Cooper et
578 al., 2019). But this work also held promise for expanding our understanding of mechanisms of
579 biofilm adaptation, given the increasing speed and economy of genotyping mutants by whole-
580 genome sequencing. As we collected these mutants and identified their genetic causes, we
581 added these discoveries into our curriculum materials and emphasized how these mutants
582 reinforced and extended our understanding of how *P. fluorescens* and its pathogenic relative *P.*
583 *aeruginosa* adapt when biofilm formation is advantageous. Mutations in the *wsp* cluster, in
584 *yfiBNR*, and in *morA* are commonly recovered in infections caused by *P. aeruginosa* (Gloag et
585 al., 2019; Malone et al., 2010; Marvig et al., 2015; Smith et al., 2006), and their recovery here
586 indicates their centrality to this lifestyle switch. In addition, our discovery of mutants in *fuzY* adds
587 to evidence that LPS alterations enhance aggregation and potentially alter susceptibility to
588 bacteriophage (Ferguson et al., 2013), and mutants in the *dsb* pathway and *bmo* highlight less
589 understood genetic pathways to biofilm production that warrant more research into how
590 *Pseudomonas* senses surfaces and initiates attachment.

The experience of offering this curriculum in subsequent years at more than 30 middle and high schools suggests broader and potentially more potent benefits, including improved student attitudes towards science and technology and greater student confidence as science learners, which we have and will report elsewhere (Quigley et al., 2025). One reason that students may begin to see themselves as scientists is the peer reinforcement from collaborating in small groups to conduct the experiments and as an entire class to discuss their findings. Likewise, often multiple classes per school participate in EvolvingSTEM, and within Pittsburgh Public Schools, twelve different schools conducted these experiments in 2024. This article synthesizes their discoveries and we hope encourages greater sharing of student discoveries among more than 2500 students annually who learn about the medical and natural relevance of microbial biofilms from our curriculum. They complete their experiments knowing that the mutants they identify may contribute to a greater understanding of how bacteria evolve in biofilms and ultimately how to manage these evolving communities.

606 **MATERIALS & METHODS**

607

608 **School bacterial growth conditions**

609 Students cultured *Pseudomonas fluorescens* strain SBW25, a plant-colonizing bacteria
610 that was isolated in 1989 from the leaf surface of a sugar beet plant grown at the University
611 Farm (Whytham, Oxford, UK) (Bailey & Thompson 1992; Rainey & Bailey 1996 Molecular
612 Microbio). Students cultured bacteria in test tubes that contained 5mL of Queen's B growth
613 media (Cooper et al. 2019, 20g Proteose Peptone No. 3, 1.5g Potassium Phosphate Dibasic,
614 25mL Glycerol, and 6mL 1M Magnesium Sulfate per liter) and a polystyrene bead and plated
615 their bead-attached bacterial populations on Half-Strength Tsoy-Agar plates (15g Tsoy and 15g
616 Agar per liter) at the beginning and end of the experiment. In addition, 25µg/mL of the broad-
617 spectrum antimicrobial triclosan was added to the media and agar plates used in the
618 experiments at SciTech and Allderdice to inhibit bacterial and fungal contamination.
619 *Pseudomonas* species are naturally resistant to triclosan, and this concentration was chosen
620 because it is used in *Pseudomonas* isolation agar (e.g., Cat# 17208 Pseudomonas Isolation
621 Agar from Millipore Sigma).

622

623 WHS students grew *P. fluorescens* cultures for 13 days at 28 °C on a roller drum under
624 biofilm selection conditions, which included 7 bead transfers. SciTech and Allderdice students
625 grew cultures for 4 days on an orbital shaker at 150rpm under biofilm selection conditions,
626 which included 3 bead transfers. SciTech students grew their cultures at 28 °C, while Allderdice
627 students grew their cultures at room temperature because they did not have an available
628 incubator.

629

630 **Genome sequencing and identification of mutants**

631 Clones were selected from the final plating day of the EvolvingSTEM classroom
632 experiment and grown overnight in 5mL QB media. DNA was extracted from 1mL of the
633 overnight culture with the DNeasy Blood and Tissue Kit (Qiagen). Illumina whole-genome
634 sequencing was performed by our laboratory to a minimum depth of 40x coverage on an
635 Illumina NextSeq500 using the methods described in Baym et al. 2015. Trimmomatic (Bolger et
636 al. 2014) was used to remove sequence adaptors, along with low-quality sequence fragments.
637 We identified mutations by comparing evolved clones to the published genome of *P. fluorescens*

638 SBW25 (NCBI Reference Sequence: NC_012660) using breseq (Deatherage and Barrick
639 2014). All sequencing data are available at NCBI Bioproject XXXXXX (SUB15372765).
640
641 The ancestral *P. fluorescens* SBW25 populations all exhibited a smooth colony
642 morphology phenotype. In comparison to the published genome sequence, the ancestor used
643 by all student populations had three intergenic mutations present in their ancestral populations:
644 (1) +G at position 45,881; (2) +C at position 985,333; and (3) $C_{5\rightarrow3}$ at position 3,447,984. The
645 ancestor used by WHS in 2015 also had a 129bp deletion at position 360,368 and an 132bp
646 deletion at position 6,223,020.
647
648 **Experimental evolution and longitudinal whole-population sequencing**
649 Populations were initiated with a single *P. fluorescens* SBW25 ancestral clone and
650 evolved for 15 days (14 transfers) in 2mL Queen's B growth medium at 28°C on an orbital
651 shaker at 150rpm. Four replicate lineages were propagated under two biofilm conditions: biofilm
652 selection + 25µg/mL triclosan and biofilm selection without triclosan. Biofilm lineages were
653 propagated using four beads each (following the methods of (Santos-Lopez et al., 2019;
654 Scribner et al., 2020). After 24 hours growth, one bead was transferred to a new test tube with
655 three new beads.
656 To perform whole-population sequencing, we collected bead-attached bacteria on days
657 3 and 15 by transferring two beads from each population to a tube with 1.2mL PBS, which was
658 vortexed for 2 minutes to release bacteria from the beads. 500uL was immediately centrifuged
659 for 10 minutes at 14,000rpm, the supernatant was removed, and pellets were stored at -20C for
660 DNA extraction. Sequencing libraries were prepared to a minimum read depth of 150x coverage
661 and analyzed as above with the additional "-p" polymorphism flag in breseq to characterize all
662 reliable mutations at intermediate frequencies in these populations.
663
664 **Motility Assays**
665 Assays were performed as described in Filloux and Ramos (2014). Images were
666 analyzed with FIJI (Schindelin et al., 2012). For swarming motility, we grew 6-hour cultures in
667 LB-Lennox Broth (10g Tryptone, 5g Yeast Extract, 5g NaCl per L) at 28°C, 150rpm, then
668 inoculated Swarming Motility Agar Plates (0.6% agar, 1x M8 solution, 0.2% glucose, 0.5%
669 casamino acids, 1mM $MgSO_4$) with 2.5µL culture pipetted onto the center of the plate, at the

670 surface of the agar. Plates were incubated upright at room temperature (~22°C) for 16-24 hours
671 and photographed. For swimming motility, we grew 6-hour cultures of *P. fluorescens* in LB-
672 Lennox Broth at 28C, 150rpm, transferred 100μL to a 1.5mL microcentrifuge tube, dipped a
673 200uL pipette tip into the culture and used this to stab into the center of Swimming Motility Agar
674 Plates (same recipe as Swarming Motility Plates, but with 0.3% agar). Plates were incubated
675 upright at room temperature (~22°C) for 16-24 hours and photographed. For twitching motility,
676 we stabbed a match-head sized inoculum from a 2-day old streak plate into the center of an LB-
677 Lennox Agar Plate (10g Tryptone, 5g Yeast Extract, 5g NaCl, 10g Agar, 0.5g Tetrazolium Red,
678 per L) all the way down to the plastic. Plates were inverted and stored in stacks of 3 or less in a
679 plastic box lined with wet paper towels at 28°C with box lid slightly ajar for 24 hours and
680 photographed.
681
682 **Biofilm assays**
683 Our biofilm assay is based on the bead model developed by our lab for studying biofilm
684 formation and evolution. Bacterial cultures were inoculated in triplicate in 2 mL of Queen's B
685 media and two plastic beads (Cospheric, Polystyrene Spheres, 7.00mm +/- 0.025mm) and
686 grown overnight at 150 rpm on an orbital shaker at 28°C. Each culture was sonicated for 10
687 seconds at 30% amplitude and used to inoculate two new cultures at a 1:100 dilution in QB both
688 with and without 30 μg/mL triclosan and two polystyrene beads. Cultures were then grown for
689 24 hours on an orbital shaker at 28°C, 150 rpm, serial diluted, and plated. Biofilm formation was
690 quantified by transferring one of the two beads to a single well of a 24-well plate with 1.5mL of
691 an 0.1% crystal violet solution and incubated at room temperature for 15 minutes. The bead was
692 then washed three times in water for one minute each time to remove excess crystal violet.
693 Biofilm-bound crystal violet was then solubilized by vortexing the bead for 2 minutes in a 2mL
694 tube filled with 1mL solubilization solution: 95% ethanol, 4.95% water, 0.05% Triton X-100. The
695 concentration of crystal violet was measured at an absorbance wavelength of 590 nm (OD590).
696 Total colony forming units per bead were determined by serial diluting and plating bacteria
697 attached to the second bead. We adopted this method to (1) more accurately represent the
698 conditions in which we grow biofilms in our experiments and (2) allow us to differentiate
699 between total biofilm production and bacterial attachment to the bead. As an indicator of EPS
700 production, we plated mutants on half-strength T-Soy Agar plates (15g Tsoy, 15g Agar, 0.02g

701 Congo Red, 0.0075g Brilliant Blue per liter) and visually assessed dye uptake, where dark red
702 colonies indicate EPS overproduction.
703
704 **Intracellular cyclic di-GMP Assay**
705 The *P. fluorescens* ancestor and biofilm-adapted mutants were transformed with the
706 cyclic di-GMP reporter plasmid, pCdrA-gfpC (Addgene plasmid #111614) (Rybtke et al., 2012).
707 The reporter transcriptionally fuses the *P. aeruginosa* PA01 *cdrA* promoter, which is responsive
708 to cyclic di-GMP, to genes encoding green fluorescent protein. Starter cultures of each
709 transformed *P. fluorescens* genotype and an untransformed ancestor control were grown in their
710 own cultures of 2 mL of Queen's B media at 28°C on an orbital shaker at 150 rpm for 24 hours.
711 Following this, experimental cultures containing 4 mL of Queen's B media were inoculated with
712 10 μL of a given starter culture and incubated at 28°C on an orbital shaker at 180 rpm for 24
713 hours. After incubation, a 100 μL sample of each experimental culture was used to capture
714 fluorescence intensity and OD_{600}. Cyclic di-GMP levels at 24 hours were calculated by
715 $\ln(RFI)/\ln(ROD_{600})$, where RFI is relative fluorescence intensity (the ratio of absolute
716 fluorescence intensity of experimental to control culture), and ROD_{600} is relative optical density
717 (the ratio of absolute optical density at a wavelength of 600 nm of a bacterial culture to fresh
718 media).
719
720 **Construction of fluorescently tagged *P. fluorescens* strains**
721 A single colony of *P. fluorescens* was inoculated into 5 ml QB and grown overnight to stationary
722 phase. One mL of culture was pelleted by centrifugation and washed twice with 300 mM
723 sucrose. After resuspending the pellet in 100 uL of 300 mM sucrose, 5 uL pTNS3 and 5 uL of
724 the desired pBT plasmid (Table S3) were added and the suspension was incubated at room
725 temperature for 5 minutes. The suspension was then transferred to an electroporation cuvette (2
726 mm gap) and pulsed at 2.5 kV. Cells were recovered in 1 mL LB and transformants were
727 selected on LB agar + 30 ug/mL gentamicin at 28˚C.
728
729 **Confocal microscopy**
730 *P. fluorescens* strains expressing eGFP or mCherry were pre-cultured for 24 hours in
731 glass-bottom plates containing 2 mL of Queen's B media and shaken on an orbital shaker at a
732 speed of 125 rpm. Biofilms generated by *P. fluorescens* were expected to attach to the surface

733 of the glass. After pre-culture, the old media in the plates were removed by pipetting, and the
734 biofilms were washed twice with 1 mL of PBS to remove excess planktonic bacterial cells.
735 Following the washing step, 1 mL of fresh PBS was added to each glass-bottom plate to
736 maintain the survival and limit the growth of bacterial cells within the biofilm. Images were
737 captured at 400× magnification in both eGFP and mCherry channels on an Olympus FV-1000
738 confocal microscope. Z-stack images spanned from the bottom to the top of the biofilms. Image
739 processing was conducted using ImageJ (Schindelin et al., 2012) and BiofilmQ (Hartmann et al.,
740 2021).
741
742 **Multi-genotype competition assay**
743 We created mixed populations of bacteria by combining a representative mutant of *bmo*
744 (PFLU0185) (with a single nucleotide insertion resulting in a premature stop codon truncating
745 both the DGC and PDE domains), wrinkly (*wspF* Q185*) and fuzzy (*fuzY* Q11*) mutants, along
746 with a lac-marked *P. fluorescens* SBW25 ancestor. All four clones were used to inoculate
747 cultures containing 2mL QB and 2 beads and grown overnight at 28°C on an orbital shaker at
748 150rpm. Both beads were then transferred to 1.5mL QB in small glass tubes and vortexed for 2
749 minutes and this mixture was used to make freezer stocks. Bacteria from a portion of one
750 freezer stock was diluted in QB and 50uL of this dilution was transferred to 6 replicate
751 populations containing 2mL QB and 4 beads. Starting frequencies of each mutant and ancestor
752 were determined by diluting a spread-plating from each starting culture. Populations were then
753 evolved for 4 days (3 transfers) in 2mL Queen's B growth medium at 28°C on an orbital shaker
754 at 150rpm. Every 24 hours, one bead was transferred to a new test tube with three new beads
755 and all newly colonized beads were vortexed for 2 minutes, diluted, and spread-plated to count
756 changes in colony phenotypes over time.
757
758 **ACKNOWLEDGEMENTS**
759 We thank Tyler McAloon and Erin Nawrocki for technical support. We appreciate the
760 commitment of dozens of teachers and thousands of students to implement this curriculum,
761 isolate these mutants, and inspire this research. This work was supported by SEPA
762 R25AI180989 from the NIH, by BIORETS DBI-2147075 from the NSF, and by the Dean's office
763 from the University of Pittsburgh, School of Medicine.
764

765 **Table 1.** Genotypes of *P. fluorescens* mutants determined by WGS that were isolated based on
766 colony phenotype by students in different schools (ST, WHS, A, or Lab = our research lab).
767 *denotes presence of secondary mutations, see Table S2 for details. #denotes representative
768 mutant used in phenotypic studies
769

School (count)	Phenotype	Position (nt)	Mutation	Annotation	Gene
ST#	smooth	210,961	+T	coding (565/1989 nt)	*PFLU0185 (bmo)*
ST	smooth	211,021	C→T	Q209* (CAG→TAG)	*PFLU0185 (bmo)*
ST*	smooth	211,277	+A	coding (881/1989 nt)	*PFLU0185 (bmo)*
ST	smooth	212,132	Δ210 bp	coding (1736-1945/1989 nt)	*PFLU0185 (bmo)*
ST / WHS*	wrinkly	1,353,115	Δ84 bp	coding (846-929/1623 nt)	*PFLU1219 (wspA)*
WHS	wrinkly	1,353,408	T→C	V380A(GTG→GCG)	*PFLU1219 (wspA)*
ST / WHS (2)	wrinkly	1,353,411	C→T	A381V (GCC→GTC)	*PFLU1219 (wspA)*
ST	wrinkly	1,355,373	Δ335 bp	fusion of 2 predicted ORFs	*[PFLU1221(wspC)] –[PFLU1222(wspD)]*
WHS	wrinkly	1,358,709	G→C	A32P (GCC→CCC)	*PFLU1224 (wspF)*
WHS (3)*	wrinkly	1,358,766	Δ15bp	coding(151-165/1011nt)	*PFLU1224 (wspF)*
WHS (3)	wrinkly	1,358,780	$(CTGATGG\ ACCTGATC)_{1\rightarrow2}$	coding (165/1011 nt)	*PFLU1224 (wspF)*
WHS	wrinkly	1,358,846	Δ18bp	coding(231-248/1011nt)	*PFLU1224 (wspF)*
WHS	wrinkly	1,358,893	Δ27 bp	coding (278-304/1011 nt)	*PFLU1224 (wspF)*
WHS (3)	wrinkly	1,358,989	+A	coding (374/1011 nt)	*PFLU1224 (wspF)*
WHS	wrinkly	1,359,085	G→T	G157V (GGC→GTC)	*PFLU1224 (wspF)*
ST# / WHS (2)*	wrinkly	1,359,168	C→T	Q185* (CAG→TAG)	*PFLU1224 (wspF)*
WHS	wrinkly	1,359,234	+G	coding (619/1011 nt)	*PFLU1224 (wspF)*
WHS	wrinkly	1,359,292	Δ150bp	coding (677-826/1011nt)	*PFLU1224 (wspF)*
WHS	wrinkly	1,359,330	G→C	A239P (GCC→CCC)	*PFLU1224 (wspF)*
WHS (6)	wrinkly	1,359,364	G→C	R250P (CGG→CCG)	*PFLU1224 (wspF)*
WHS*	wrinkly	1,359,370	C→T	S252L (TCG→TTG)	*PFLU1224 (wspF)*
ST	wrinkly	1,359,446	Δ1 bp	coding (831/1011 nt)	*PFLU1224 (wspF)*
WHS (2)	wrinkly	1,359,495	A→C	T294P (ACC→CCC)	*PFLU1224 (wspF)*
WHS (3)	wrinkly	1,359,538	C→T	P308L(CCC→CTC)	*PFLU1224 (wspF)*
WHS	wrinkly	1,359,552	$(GCG)_{4\rightarrow3}$	coding (937-939/1011 nt)	*PFLU1224 (wspF)*
WHS	wrinkly	1,359,554	$(GCG)_{4\rightarrow5}$	coding (939/1011 nt)	*PFLU1224 (wspF)*

ST (3)	small	4,830,895	$(GCAGGC)_{2\rightarrow1}$	coding (8-13/1323 nt)	*PFLU4380 (dsbS)*
ST	small	4,834,252	Δ110 bp	fusion of 2 predicted ORFS	*[PFLU4383]–[PFLU4384 (dsbG)]*
ST	wrinkly	5,707,197	G→A	Q157* (CAA→TAA)	*PFLU5211 (awsX/YfiR)*
ST	wrinkly	5,707,256	A→C	I137S (ATC→AGC)	*PFLU5211 (awsX/YfiR)*
WHS*	wrinkly	5,707,317	Δ33bp	coding (317-349/573nt)	*PFLU5211 (awsX/YfiR)*
WHS	wrinkly	5,707,334	G→T	A111E (GCG→GAG)	*PFLU5211 (awsX/YfiR)*
ST/WHS (5)*	wrinkly	5,707,411	Δ33 bp	coding (223-255/573 nt)	*PFLU5211 (awsX/YfiR)*
ST (2)	wrinkly	5,857,638	G→A	M992I (ATG→ATA)	*PFLU5329 (mwsR/morA)*
ST (3)	wrinkly	5,857,733	Δ9 bp	coding (3071-3079/3852 nt)	*PFLU5329 (mwsR/morA)*
A (3)*	wrinkly	5,858,369	C→T	A1236V (GCC→GTC)	*PFLU5329 (mwsR/morA)*
Lab#	fuzzy	541,214	C→T	Q11* (CAG→TAG)	*PFLU0478 (fuzY)*
Lab	fuzzy	541,772	Δ13 bp	coding (589-601/1149 nt)	*PFLU0478 (fuzY)*

770

771 **Table 2**. Linear regressions of frequencies of *bmo* (PFLU0185) between the ancestor (Afreq),
772 *wsp* mutant (Wfreq), and *fzy* mutant (Ffreq), as shown in Figure S4. The significant negative
773 slopes indicate competition.

Model Equation	Std. Error	t value	R-squared	p-value
Pfreq = (-0.99)Afreq + 0.91	0.07	-14.69	0.79	<0.0001
Pfreq = (-0.7)Wfreq + 0.46	0.32	-2.22	0.08	<0.05
Pfreq = (-1.84)Ffreq + 0.48	0.58	-3.14	0.15	<0.001

778

779 **Table S1.** Complete details of mutant genotypes, including secondary mutations (XLS).

780

781 **Table S2**. Details of mutations detected during the evolution experiment using population-wide
782 whole-genome sequencing (XLS)

783

784 **Table S3.** Plasmids used in this study

Name	Plasmid	Source/Reference
pTNS3	Helper plasmid for site-specific Tn7 transposition	Choi et al. (Choi et al., 2008)
pBT270	pUC18-mini-Tn7T2-PA1/04/03-Gm-GFP	Zhao et al. (Zhao et al., 2013)
pBT272	pUC18-mini-Tn7T2-PA1/04/03-Gm-TagRFP657	Zhao et al. (Zhao et al., 2013)
pBT273	pUC18-mini-Tn7T2-PA1/04/03-Gm-mTFP1	Zhao et al. (Zhao et al., 2013)
pBT276	pUC18-mini-Tn7T2-PA1/04/03-Gm-tdTomato	Zhao et al. (Zhao et al., 2013)
pBT277	pUC18-mini-Tn7T2-PA1/04/03-Gm-mCherry	Zhao et al. (Zhao et al., 2013)
pBT278	pUC18-mini-Tn7T2-PA1/04/03-Gm-mKO1	Zhao et al. (Zhao et al., 2013)
pBT279	pUC18-mini-Tn7T2-PA1/04/03-Gm-eYFP	Zhao et al. (Zhao et al., 2013)

785

786

787 **FIGURE LEGENDS**

788 **Fig. 1. Biofilm growth patterns and colony morphologies of *P. fluorescens* SBW25**
789 **and evolved biofilm-adapted mutants.** Evolved populations often have a distinct ring of
790 biofilm at the air-liquid interface (A). The *P. fluorescens* ancestor (lac+) has blue, smooth-edged
791 circular colonies (pink circle), the *bmo* (PFLU0185) mutant has yellow, smooth-edged circular
792 colonies (orange circle), the *fuzY* mutant has large, yellow, irregular colonies (yellow circle), and
793 the *wspF* mutant has small, white, irregular colonies (purple circle) (B). Small colony variants
794 (green circle) can be distinguished from their ancestor (pink circle) by their significantly smaller
795 size (B).
796

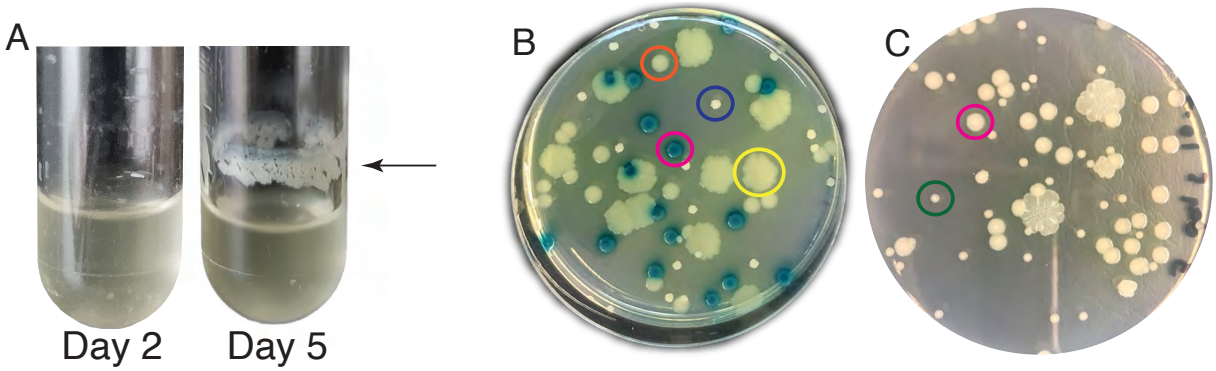

797
798
799

800 **Fig. 2. Wrinkly colony phenotypes are caused by mutations in the *wsp*, *yfiBNR*,**
801 **and *morA* pathways.** Mutations are shown as black bars below the gene diagrams. When
802 multiple independent mutations occurred, their counts are in parentheses. Mutations in *wspF*
803 (31 in total) are too numerous to display. DGC domains are indicated with diagonal hatching;
804 PDE domains are indicated with cross hatching. Genome positions of the beginning and end of
805 each operon/gene are indicated above the gene diagrams. Table 1 and Table S1 contain a
806 complete list of mutations. All mutations are predicted to cause constitutive activation of a DGC,
807 increasing cyclic di-GMP synthesis.

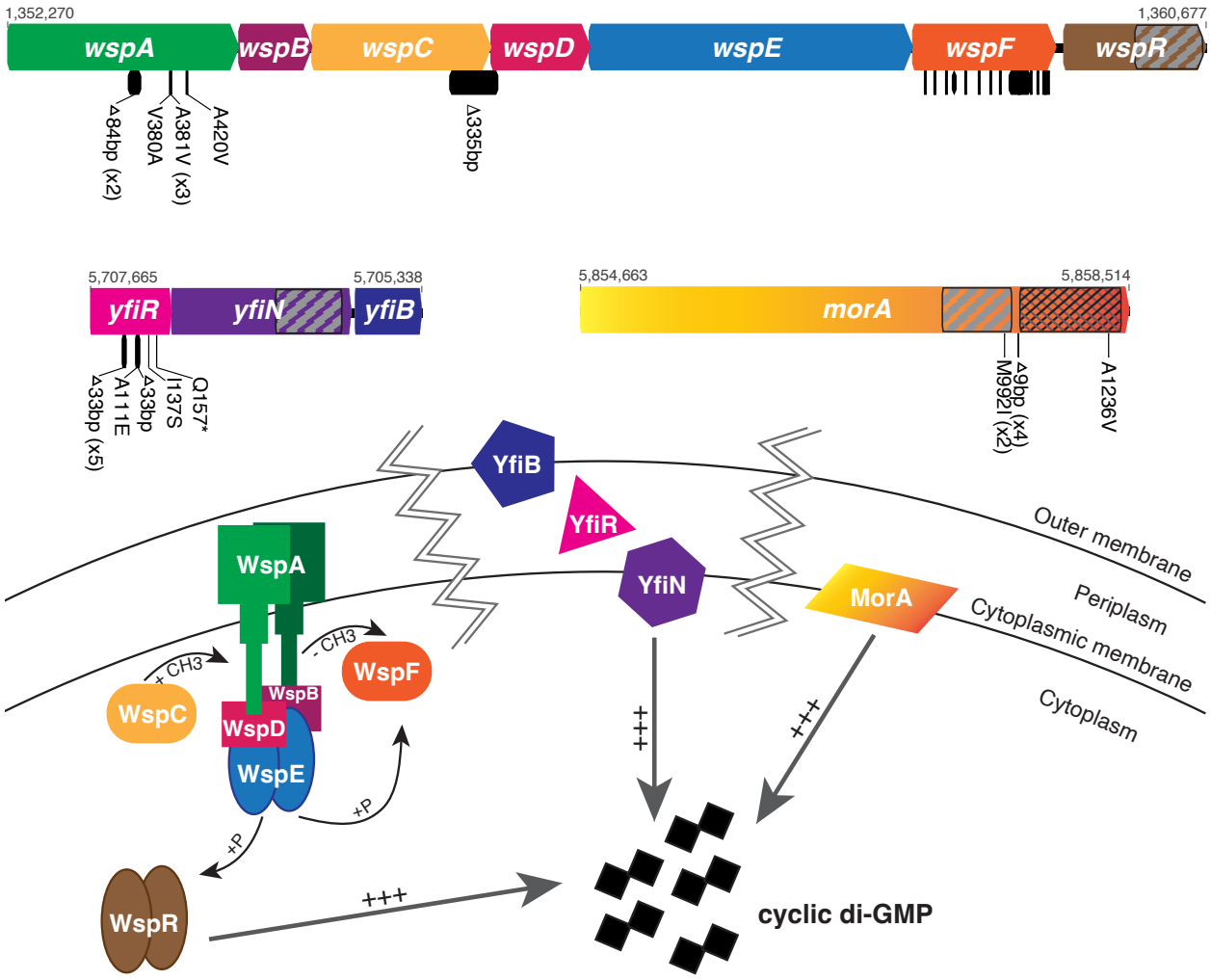

808
809

810 **Fig. 3. Biofilm adaptations caused by mutations in LPS, disulfide bond formation,**
811 **and a novel regulator of cyclic-di-GMP.** Mutations are shown as black bars below the gene
812 diagrams. When multiple independent mutations occurred, their counts are in parentheses.
813 DGC domains are indicated with diagonal hatching; PDE domains are indicated with cross
814 hatching. Genome positions of the beginning and end of each operon/gene are indicated above
815 the gene diagrams. Mutations in *bmo* (PFLU0185) are predicted to increase basal levels of
816 cyclic di-GMP (A). Mutations in *fuzY* are predicted to modify LPS O-antigens (B). Mutations in
817 *dsb* genes are predicted to cause misfolded periplasmic proteins. Table 1 and Table S1 provide
818 mutation details.

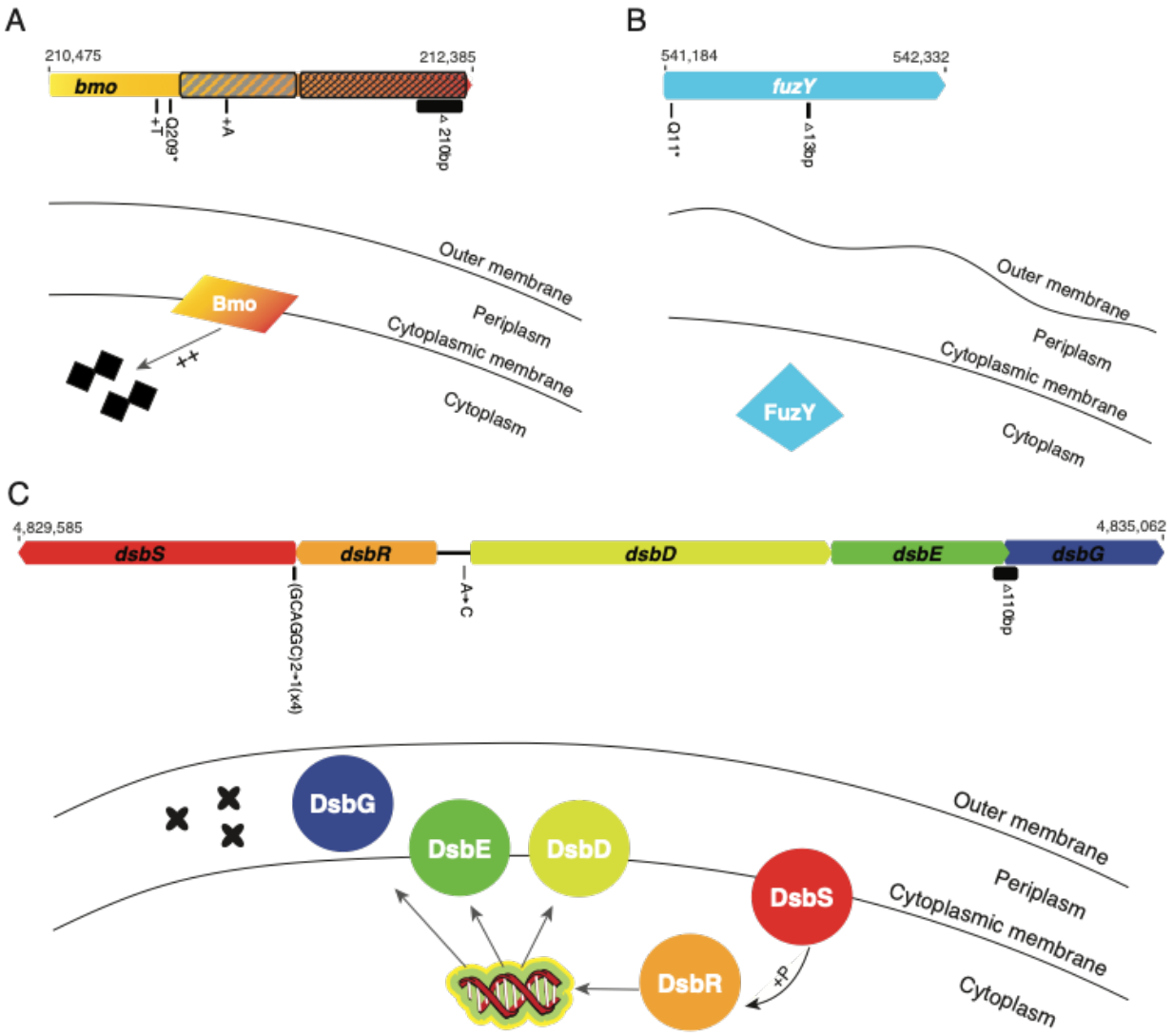

819
820

821 **Fig. 4. Dynamics of evolved phenotypes and genotypes during 15 days of**
822 **experimental biofilm selection.** Populations were grown for 15 days in QB media with or
823 without triclosan with four plastic beads and passaged every 24 hours by transferring one bead
824 into fresh media with three new beads. Bead-attached populations were plated on days 4, 8, 11,
825 and 15 and contained colonies with fuzzy, small, smooth, and wrinkly phenotypes (A). Whole-
826 genome, whole-population sequencing was performed on days 3 and 15. Points include the
827 cumulative frequency of mutations identified in each gene (B). A complete list of mutations can
828 be found in Supplemental Table 1.

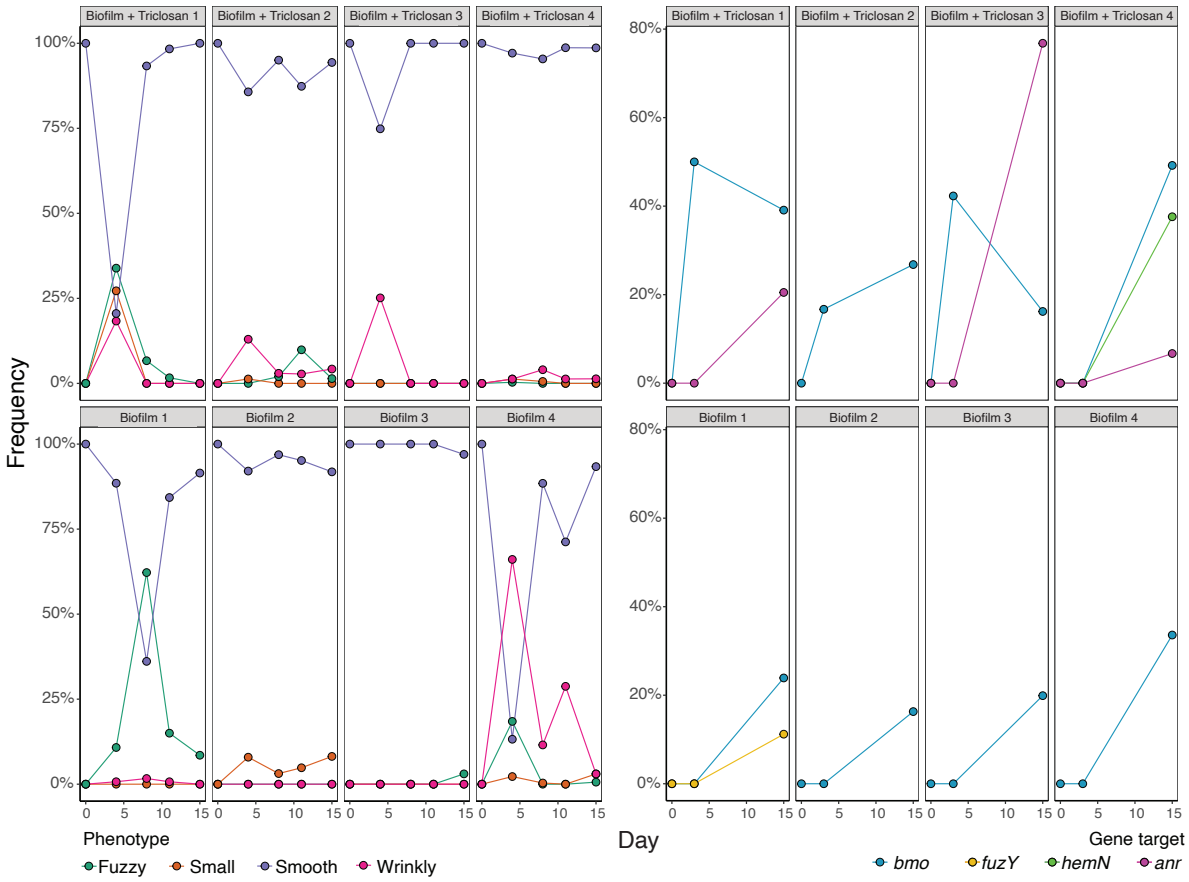

829

830 **Fig. 5. Biofilm-related phenotypes of *P. fluorescens* mutants**. Swarming motility (A)
831 and swimming motility (B) show reduced levels compared to the ancestor. Biofilm production
832 measured by attached colony forming units (C) and by crystal violet absorbance at 590nm (D).
833 Points are the average of three measurements recorded for each replicate. Results in QB media
834 are similar but more pronounced with the addition of triclosan. Relative cyclic di-GMP production
835 from a fluorescent reporter (E) is reported as ln(RFI)/ln(ROD600), where RFI is relative
836 fluorescence intensity and ROD600 is relative optical density. In all panels, mean values are
837 indicated by diamonds, and outliers are indicated by an open circle. Statistical comparisons
838 were conducted by one-way ANOVA with a Games-Howell post hoc test with p = 0.05, with
839 letters at the top of each panel indicating statistically distinct groupings.

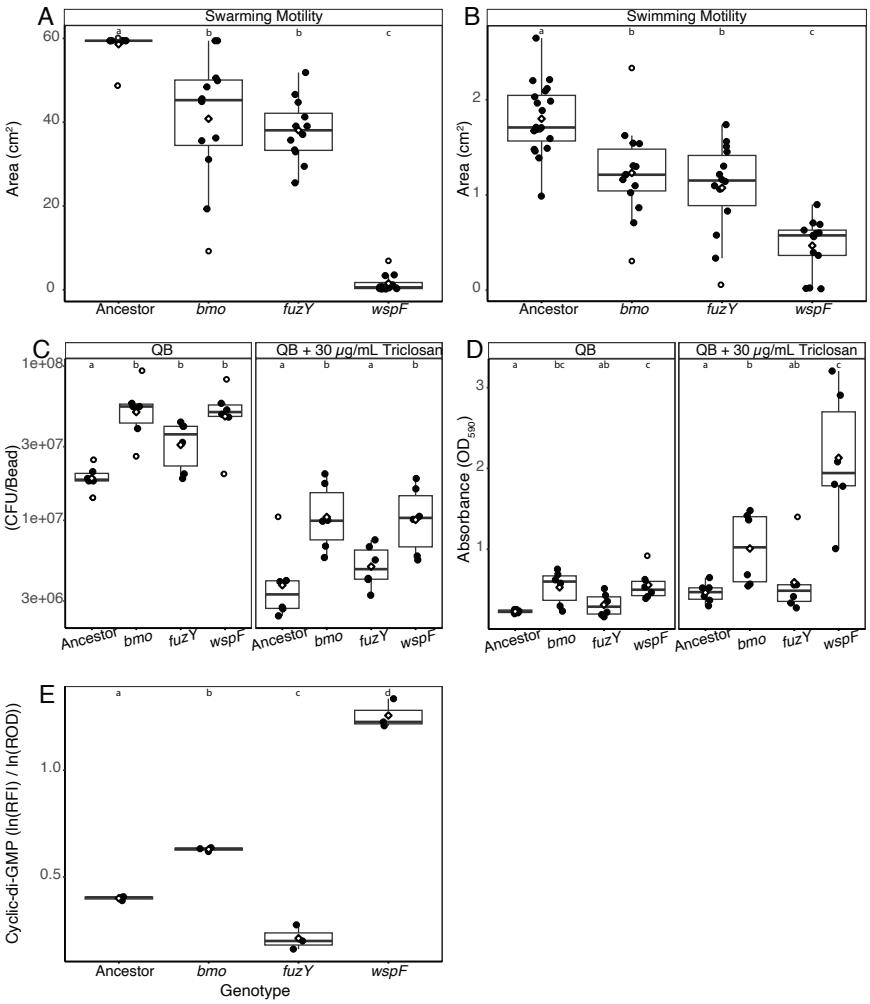

840
841

842 **Fig. 6. Confocal microscopy of representative *P. fluorescens* mutants shows**
843 **differentiated biofilm phenotypes.**. Ancestor (a), fuzY (c) and *wspF* (d) are tagged with eGFP
844 and *bmo* (b) is tagged with mCherry. Both Ancestor and *bmo* exhibit uniform biofilm structure.
845 The *fuzY* biofilm is composed of many aggregates. The *wspF* biofilm was in small clusters and
846 was not spatially contiguous on the glass surface, but generated large aggregates in liquid
847 media that were more likely to attach on plastic surfaces (not shown).

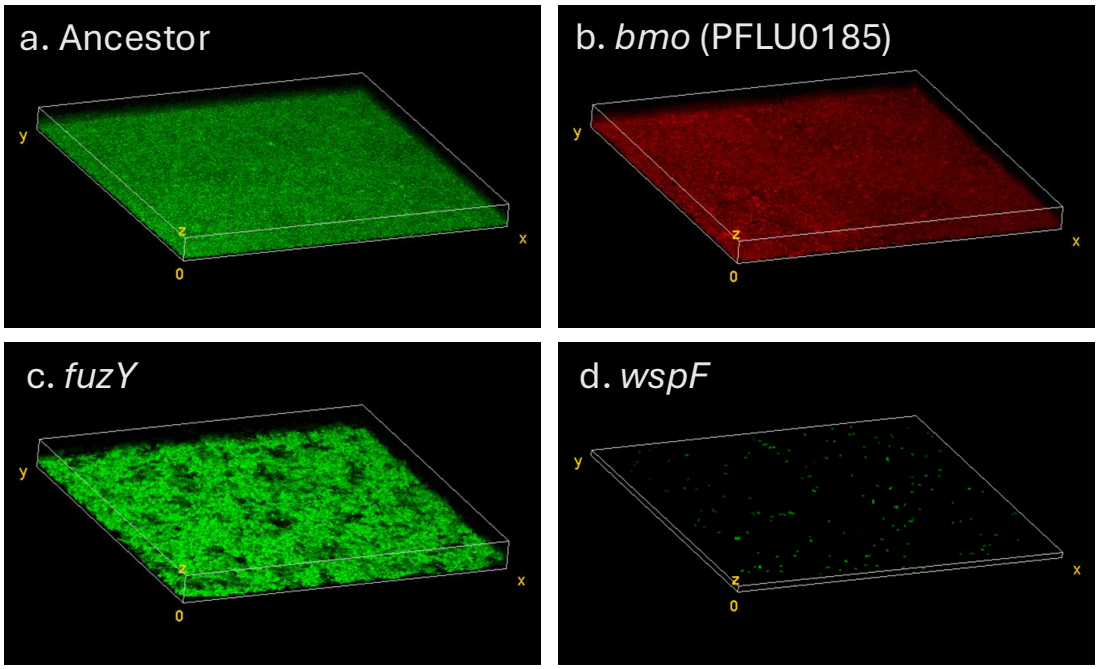

848
849

850 **Fig. 7. Ecological dynamics of constructed communities indicate multi-niche**
851 **selection.** Six populations containing equal volumes of representative, biofilm-adapted loss-of-
852 function mutants in *bmo* (PFLU0185), *fuzY*, and *wspF* were propagated in the biofilm bead
853 model and plated daily to assess frequencies. All mutants persisted, with *fuzY* and *wspF*
854 declining rapidly in frequency and *bmo* and the ancestor fluctuating at intermediate frequencies
855 and opposite trajectories.

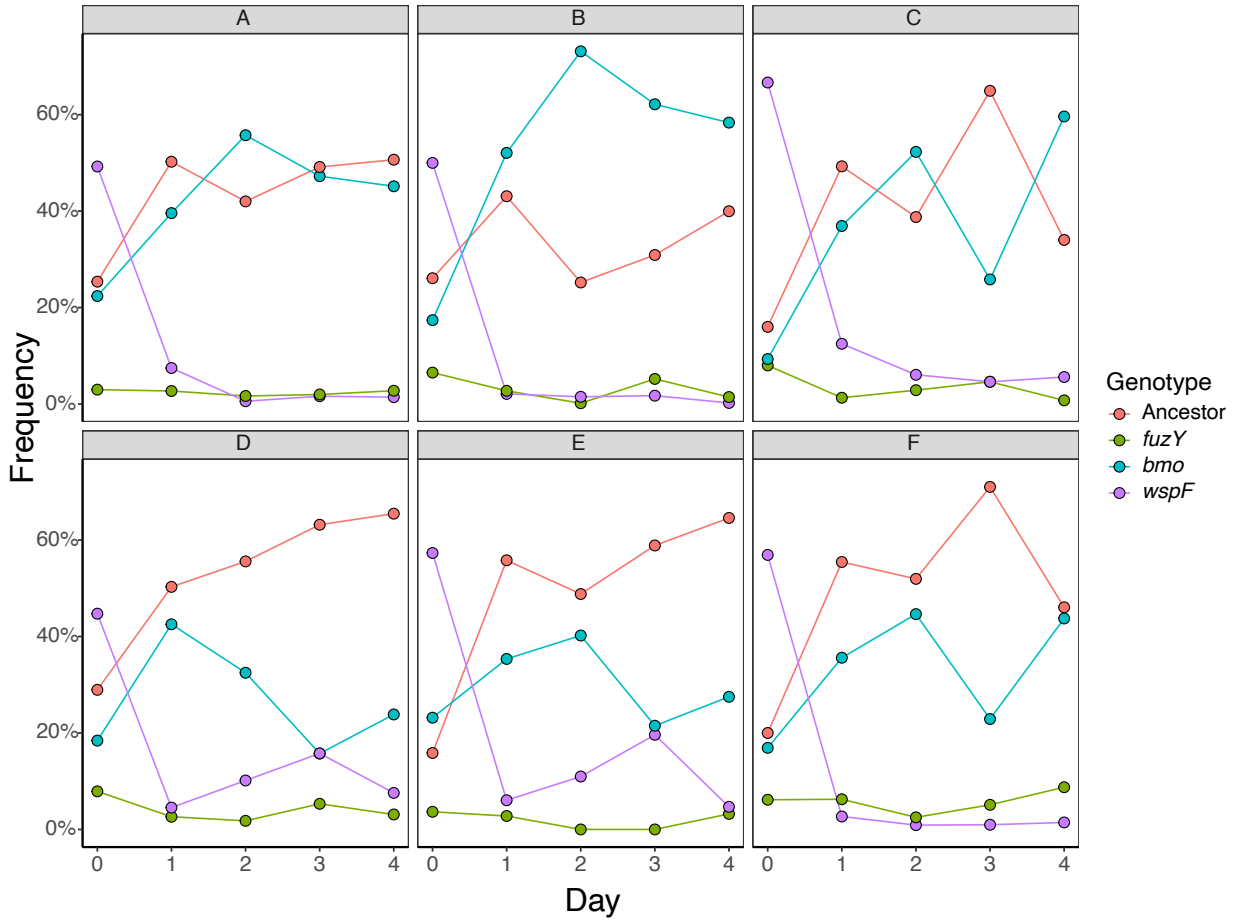

856
857

858 **Fig. S1. *Pseudomonas fluorescens* lacks twitching motility**. Twitching motility was
859 measured on LB-Lennox Agar Plates after 24 hours of growth. PA01 (A) exhibits a twitching
860 phenotype, indicated by the halo surrounding the dark red colony in the center of the plate
861 where inoculation occurred. *P. fluorescens* ancestor (B), *pflu0185* mutants (C), *fuzY* mutants
862 (D), and *wspF* mutants (E) show no signs of twitching motility as all four genotypes lack a halo
863 surrounding the inoculation point.

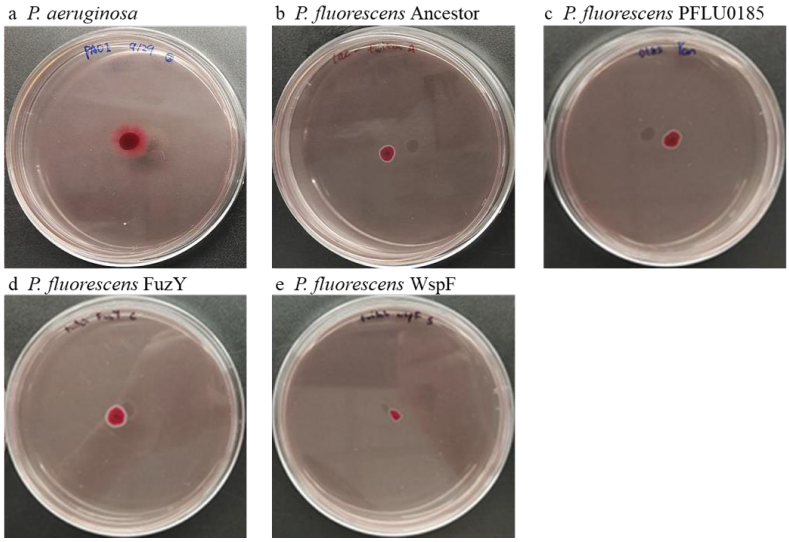

864
865
866

867 **Fig. S2. Planktonic growth is inhibited by triclosan.**

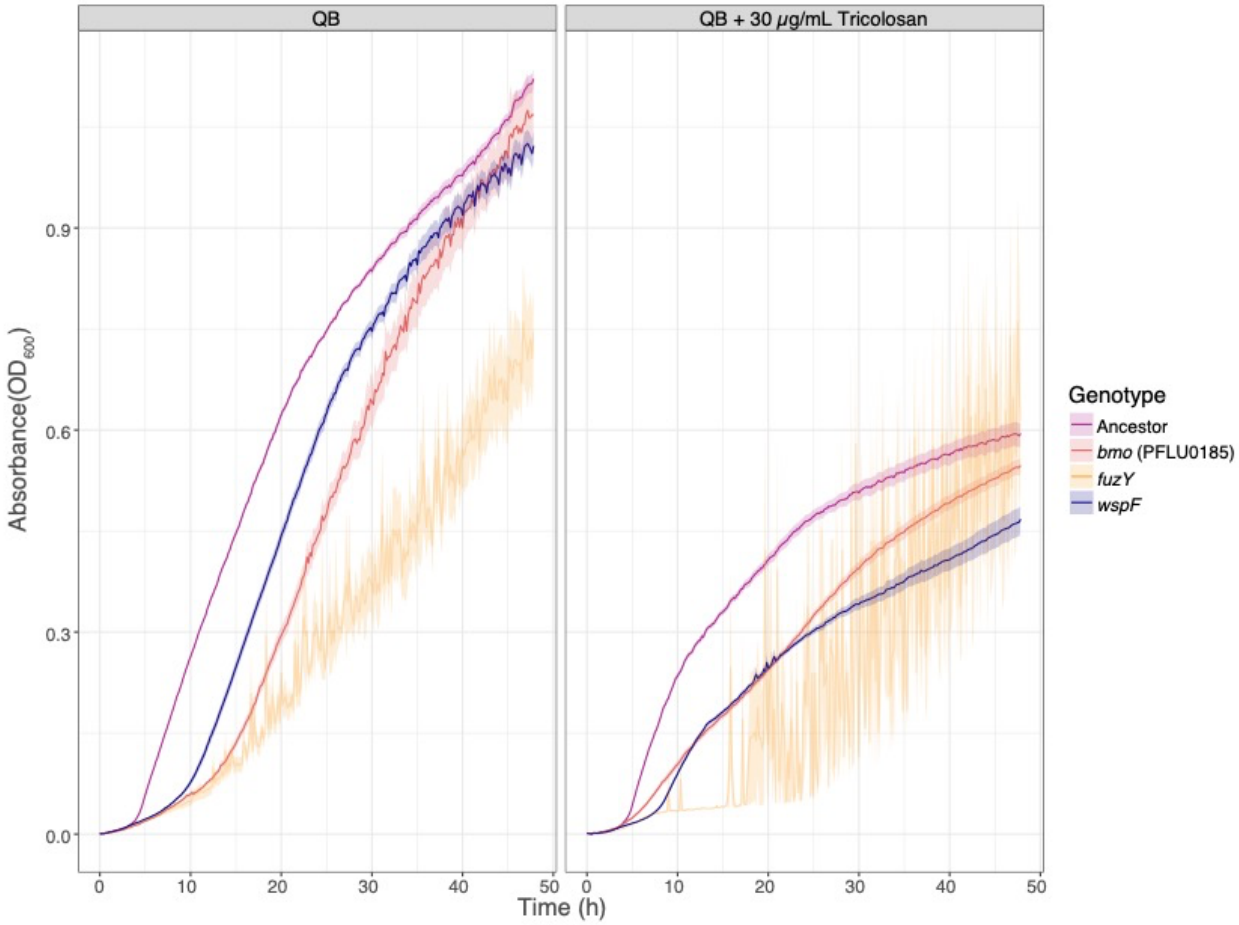

868

869 **Fig. S3. Confocal microscopy of representative *P. fluorescens* mutants mixed in**
870 **pairs shows differentiated biofilm phenotypes**. Text color of labels indicates fluorescent
871 marker in that genotype; red = mCherry, green = eGFP.

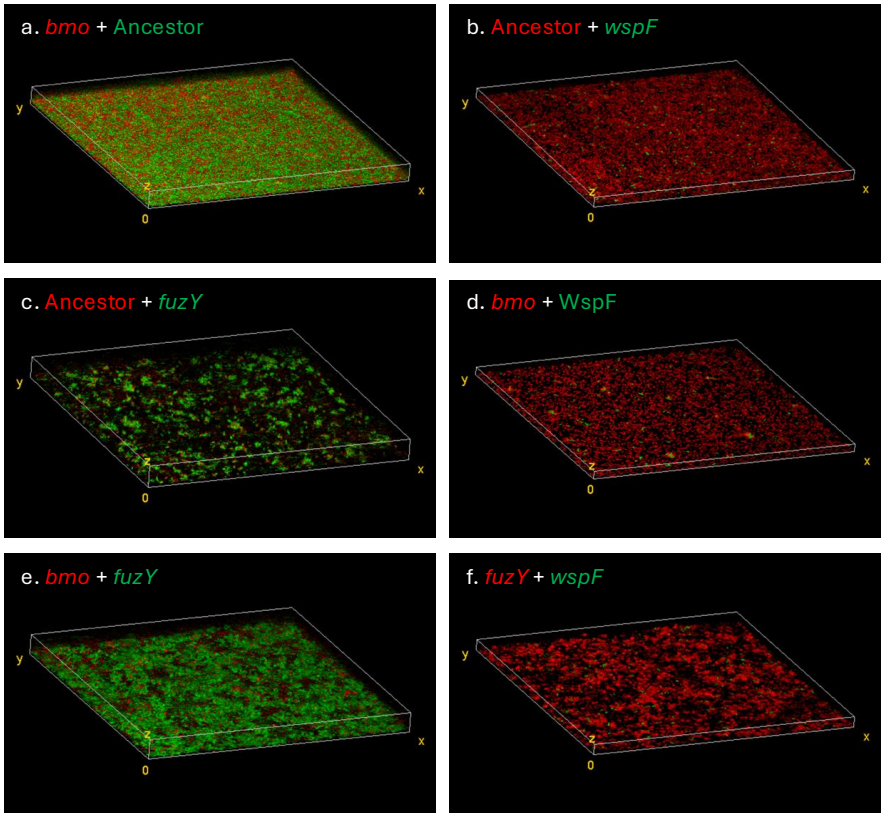
a. bmo + Ancestor
b. Ancestor + wspF
c. Ancestor + fuzY
d. bmo + WspF
e. bmo + fuzY
f. fuzY + wspF

874 **Fig. S4. Linear regressions of *bmo* frequencies, as compared to ancestor (A),**
875 ***wspF* (B), and *fuzY* (C).**

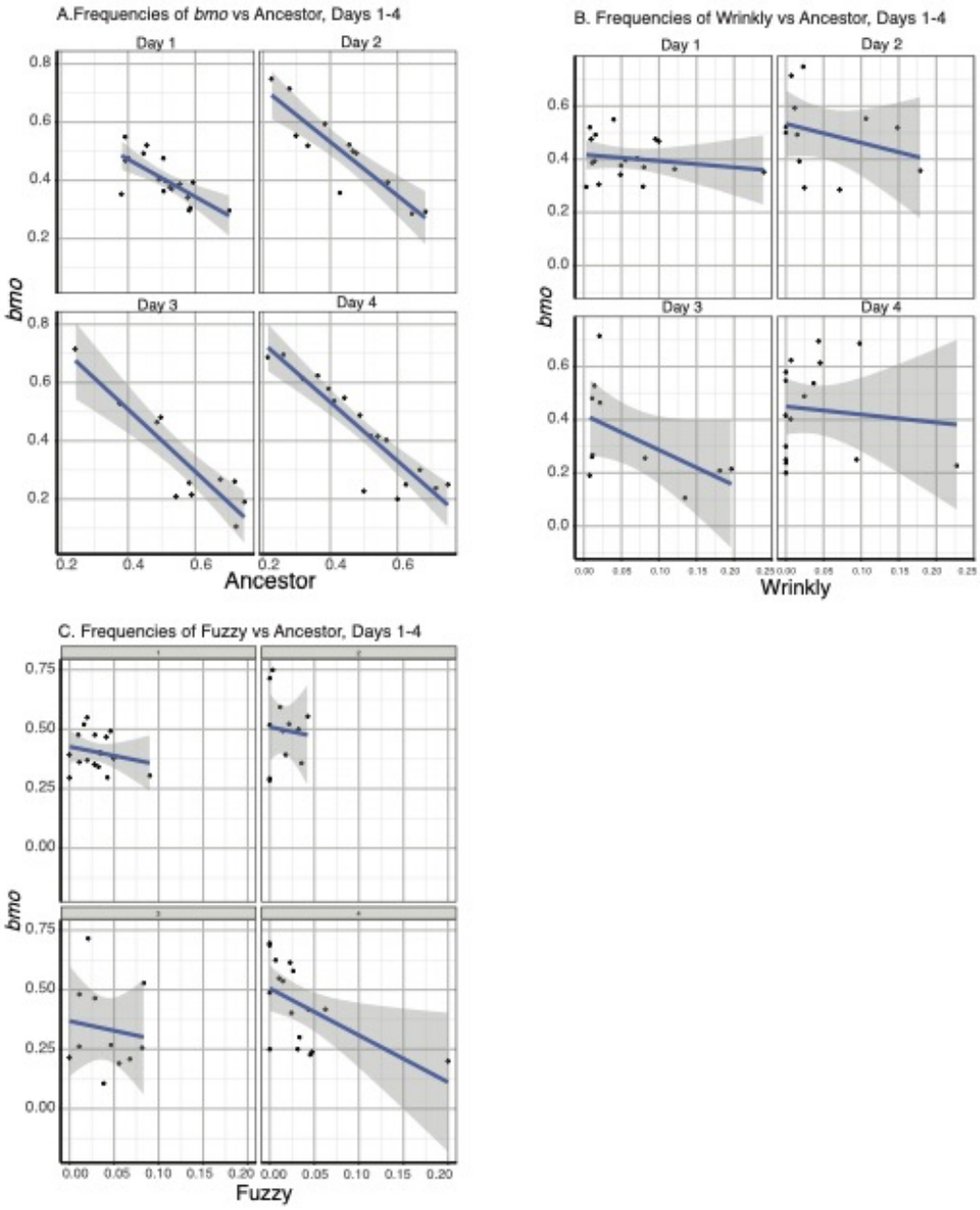

876
877

878 **Fig. S5. Colony morphology of small colony variants with mutations in *dsb* genes**

879 **and their differential uptake of Congo Red dye.**

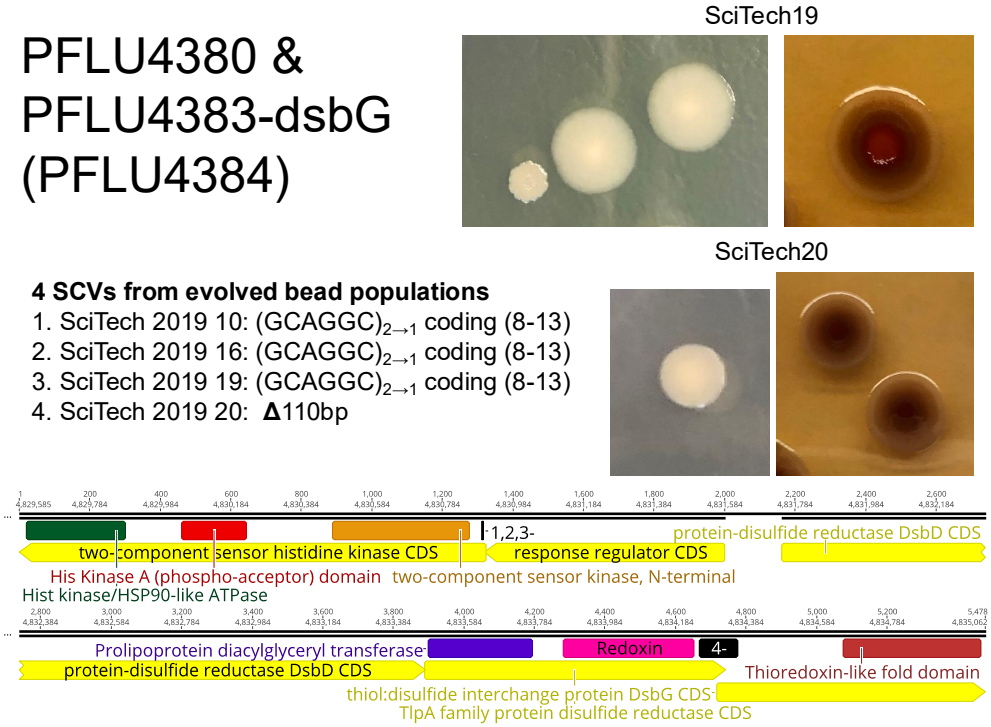

880

881

882

883 **REFERENCES**

884

885 Bader, M. W., Xie, T., Yu, C.-A., & Bardwell, J. C. A. (2000). Disulfide Bonds Are Generated by
886 Quinone Reduction *. *Journal of Biological Chemistry*, *275*(34), 26082–26088.
887 https://doi.org/10.1074/jbc.M003850200

888 Bantinaki, E., Kassen, R., Knight, C. G., Robinson, Z., Spiers, A. J., & Rainey, P. B. (2007).
889 Adaptive Divergence in Experimental Populations of Pseudomonas fluorescens. III.
890 Mutational Origins of Wrinkly Spreader Diversity. *Genetics*, *176*(1), 441–453.
891 https://doi.org/10.1534/genetics.106.069906

892 Bardwell, J. C. A., McGovern, K., & Beckwith, J. (1991). Identification of a protein required for
893 disulfide bond formation in vivo. *Cell*, *67*(3), 581–589. https://doi.org/10.1016/0092-
894 8674(91)90532-4

895 Bardwell, J. C., Lee, J. O., Jander, G., Martin, N., Belin, D., & Beckwith, J. (1993). A pathway for
896 disulfide bond formation in vivo. *Proceedings of the National Academy of Sciences*,
897 *90*(3), 1038–1042. https://doi.org/10.1073/pnas.90.3.1038

898 Berkmen, M., Boyd, D., & Beckwith, J. (2005). The Nonconsecutive Disulfide Bond of
899 Escherichia coli Phytase (AppA) Renders It Dependent on the Protein-disulfide
900 Isomerase, DsbC *. *Journal of Biological Chemistry*, *280*(12), 11387–11394.
901 https://doi.org/10.1074/jbc.M411774200

902 Brisson, D. (2018). Negative Frequency-Dependent Selection Is Frequently Confounding.
903 *Frontiers in Ecology and Evolution*, *6*. https://doi.org/10.3389/fevo.2018.00010

904 Cai, Y.-M., Yu, K.-W., Liu, J.-H., Cai, Z., Zhou, Z.-H., Liu, Y., Wang, T.-F., & Yang, L. (2022).
905 The c-di-GMP Phosphodiesterase PipA (PA0285) Regulates Autoaggregation and Pf4
906 Bacteriophage Production in Pseudomonas aeruginosa PAO1. *Applied and*
907 *Environmental Microbiology*, *88*(12), e00039-22. https://doi.org/10.1128/aem.00039-22

Caplat, P., Anand, M., & Bauch, C. (2008). Symmetric competition causes population oscillations in an individual-based model of forest dynamics. *Ecological Modelling*, *211*(3), 491–500. https://doi.org/10.1016/j.ecolmodel.2007.10.002

Chesson, P. (2000). Mechanisms of Maintenance of Species Diversity. *Annual Review of Ecology, Evolution, and Systematics*, *31*(Volume 31, 2000), 343–366. https://doi.org/10.1146/annurev.ecolsys.31.1.343

Choi, K.-H., Mima, T., Casart, Y., Rholl, D., Kumar, A., Beacham, I. R., & Schweizer, H. P. (2008). Genetic Tools for Select-Agent-Compliant Manipulation of Burkholderia pseudomallei. *Applied and Environmental Microbiology*, *74*(4), 1064–1075. https://doi.org/10.1128/AEM.02430-07

Cooper, V. S., Staples, R. K., Traverse, C. C., & Ellis, C. N. (2014). Parallel evolution of small colony variants in Burkholderia cenocepacia biofilms. *Genomics*, *104*(6, Part A), 447–452. https://doi.org/10.1016/j.ygeno.2014.09.007

Cooper, V. S., Warren, T. M., Matela, A. M., Handwork, M., & Scarponi, S. (2019). EvolvingSTEM: A microbial evolution-in-action curriculum that enhances learning of evolutionary biology and biotechnology. *Evolution: Education and Outreach*, *12*(1), 12. https://doi.org/10.1186/s12052-019-0103-4

Eilers, K., Hoong Yam, J. K., Liu, X., Goh, Y. F., To, K.-N., Paracuellos, P., Morton, R., Brizuela, J., Hui Yong, A. M., Givskov, M., Freibert, S.-A., Bange, G., Rice, S. A., Steinchen, W., & Filloux, A. (2024). The dual GGDEF/EAL domain enzyme PA0285 is a *Pseudomonas* species housekeeping phosphodiesterase regulating early attachment and biofilm architecture. *Journal of Biological Chemistry*, *300*(2), 105659. https://doi.org/10.1016/j.jbc.2024.105659

Eilers, K., Kuok Hoong Yam, J., Morton, R., Mei Hui Yong, A., Brizuela, J., Hadjicharalambous, C., Liu, X., Givskov, M., Rice, S. A., & Filloux, A. (2022). Phenotypic and integrated analysis of a comprehensive Pseudomonas aeruginosa PAO1 library of mutants lacking cyclic-di-GMP-related genes. *Frontiers in Microbiology*, *13*. https://doi.org/10.3389/fmicb.2022.949597

Eilers, K., Yam, J. K. H., Liu, X., Goh, Y. F., To, K.-N., Paracuellos, P., Morton, R., Brizuela, J., Yong, A. M. H., Givskov, M., Freibert, S.-A., Bange, G., Rice, S. A., Steinchen, W., & Filloux, A. (2024). The dual GGDEF/EAL domain enzyme PA0285 is a Pseudomonas species housekeeping phosphodiesterase regulating early attachment and biofilm architecture. *Journal of Biological Chemistry*, *300*(2). https://doi.org/10.1016/j.jbc.2024.105659

Ellis, C. N., Traverse, C. C., Mayo-Smith, L., Buskirk, S. W., & Cooper, V. S. (2015). Character displacement and the evolution of niche complementarity in a model biofilm community. *Evolution; International Journal of Organic Evolution*, *69*(2), 283–293. https://doi.org/10.1111/evo.12581

Ferguson, G. C., Bertels, F., & Rainey, P. B. (2013). Adaptive Divergence in Experimental Populations of Pseudomonas fluorescens. V. Insight into the Niche Specialist Fuzzy Spreader Compels Revision of the Model Pseudomonas Radiation. *Genetics*, *195*(4), 1319–1335. https://doi.org/10.1534/genetics.113.154948

Flemming, H.-C., & Wuertz, S. (2019). Bacteria and archaea on Earth and their abundance in biofilms. *Nature Reviews Microbiology*, *17*(4), 247–260. https://doi.org/10.1038/s41579-019-0158-9

Flynn, K. M., Dowell, G., Johnson, T. M., Koestler, B. J., Waters, C. M., & Cooper, V. S. (2016). Evolution of Ecological Diversity in Biofilms of Pseudomonas aeruginosa by Altered

Cyclic Diguanylate Signaling. *Journal of Bacteriology*, *198*(19), 2608–2618. https://doi.org/10.1128/JB.00048-16

Gloag, E. S., Marshall, C. W., Snyder, D., Lewin, G. R., Harris, J. S., Santos-Lopez, A., Chaney, S. B., Whiteley, M., Cooper, V. S., & Wozniak, D. J. (2019). Pseudomonas aeruginosa Interstrain Dynamics and Selection of Hyperbiofilm Mutants during a Chronic Infection. *mBio*, *10*(4), e01698-19. https://doi.org/10.1128/mBio.01698-19

Ha, D.-G., Richman, M. E., & O'Toole, G. A. (2014). Deletion Mutant Library for Investigation of Functional Outputs of Cyclic Diguanylate Metabolism in Pseudomonas aeruginosa PA14. *Applied and Environmental Microbiology*, *80*(11), 3384–3393. https://doi.org/10.1128/AEM.00299-14

Habets, M. G. J. L., Rozen, D. E., Hoekstra, R. F., & de Visser, J. A. G. M. (2006). The effect of population structure on the adaptive radiation of microbial populations evolving in spatially structured environments. *Ecology Letters*, *9*(9), 1041–1048. https://doi.org/10.1111/j.1461-0248.2006.00955.x

Hall-Stoodley, L., Costerton, J. W., & Stoodley, P. (2004). Bacterial biofilms: From the Natural environment to infectious diseases. *Nature Reviews Microbiology*, *2*(2), 95–108. https://doi.org/10.1038/nrmicro821

Harris, K. B., Flynn, K. M., & Cooper, V. S. (2021). Polygenic Adaptation and Clonal Interference Enable Sustained Diversity in Experimental Pseudomonas aeruginosa Populations. *Molecular Biology and Evolution*, msab248. https://doi.org/10.1093/molbev/msab248

Hartmann, R., Jeckel, H., Jelli, E., Singh, P. K., Vaidya, S., Bayer, M., Rode, D. K. H., Vidakovic, L., Díaz-Pascual, F., Fong, J. C. N., Dragoš, A., Lamprecht, O., Thöming, J.

G., Netter, N., Häussler, S., Nadell, C. D., Sourjik, V., Kovács, Á. T., Yildiz, F. H., & Drescher, K. (2021). Quantitative image analysis of microbial communities with BiofilmQ. *Nature Microbiology*, *6*(2), 151–156. https://doi.org/10.1038/s41564-020-00817-4

Henriksen, N. N. S. E., Hansen, M. F., Kiesewalter, H. T., Russel, J., Nesme, J., Foster, K. R., Svensson, B., Øregaard, G., Herschend, J., & Burmølle, M. (2022). Biofilm cultivation facilitates coexistence and adaptive evolution in an industrial bacterial community. *Npj Biofilms and Microbiomes*, *8*(1), 1–8. https://doi.org/10.1038/s41522-022-00323-x

Hiniker, A., & Bardwell, J. C. A. (2004). In Vivo Substrate Specificity of Periplasmic Disulfide Oxidoreductases *. *Journal of Biological Chemistry*, *279*(13), 12967–12973. https://doi.org/10.1074/jbc.M311391200

Jenal, U., Reinders, A., & Lori, C. (2017). Cyclic di-GMP: Second messenger extraordinaire. *Nature Reviews Microbiology*, *15*(5), 271–284. https://doi.org/10.1038/nrmicro.2016.190

Kassen, R., & Rainey, P. B. (2004). The Ecology and Genetics of Microbial Diversity. *Annual Review of Microbiology*, *58*(Volume 58, 2004), 207–231. https://doi.org/10.1146/annurev.micro.58.030603.123654

Kessler, C., & Kim, W. (2022). Identification of Cyclic-di-GMP-Modulating Protein Residues by Bidirectionally Evolving a Social Behavior in Pseudomonas fluorescens. *mSystems*, *7*(5), e00737-22. https://doi.org/10.1128/msystems.00737-22

Kessler, C., Mhatre, E., Cooper, V., & Kim, W. (2021). Evolutionary Divergence of the Wsp Signal Transduction Systems in Beta- and Gammaproteobacteria. *Applied and Environmental Microbiology*. https://doi.org/10.1128/AEM.01306-21

Koza, A., Kuśmierska, A., McLaughlin, K., Moshynets, O., & Spiers, A. J. (2017). Adaptive radiation of Pseudomonas fluorescens SBW25 in experimental microcosms provides an understanding of the evolutionary ecology and molecular biology of A-L interface biofilm

1003 formation. *FEMS Microbiology Letters*, *364*(12), fnx109.
1004 https://doi.org/10.1093/femsle/fnx109
1005 Lam, J. S., Taylor, V. L., Islam, S. T., Hao, Y., & Kocíncová, D. (2011). Genetic and Functional
1006 Diversity of Pseudomonas aeruginosa Lipopolysaccharide. *Frontiers in Microbiology*, *2*.
1007 https://doi.org/10.3389/fmicb.2011.00118
1008 Lau, P. C. Y., Lindhout, T., Beveridge, T. J., Dutcher, J. R., & Lam, J. S. (2009). Differential
1009 Lipopolysaccharide Core Capping Leads to Quantitative and Correlated Modifications of
1010 Mechanical and Structural Properties in Pseudomonas aeruginosa Biofilms. *Journal of*
1011 *Bacteriology*, *191*(21), 6618–6631. https://doi.org/10.1128/jb.00698-09
1012 Laventie, Benoit-Joseph, J., Urs. (2020). Surface Sensing and Adaptation in Bacteria. *Annual*
1013 *Review of Microbiology*, *74*(1), 735–760.
1014 Lerouge, I., & Vanderleyden, J. (2002). O-antigen structural variation: Mechanisms and possible
1015 roles in animal/plant–microbe interactions. *FEMS Microbiology Reviews*, *26*(1), 17–47.
1016 https://doi.org/10.1111/j.1574-6976.2002.tb00597.x
1017 Levins, R. (1963). Theory of Fitness in a Heterogeneous Environment. II. Developmental
1018 Flexibility and Niche Selection. *The American Naturalist*, *97*(893), 75–90.
1019 https://doi.org/10.1086/282258
1020 Li, S., Li, T., Teng, X., Lou, X., Xu, Y., Zhang, Q., & Bartlam, M. (2018). Structural analysis of
1021 activating mutants of YfiB from Pseudomonas aeruginosa PAO1. *Biochemical and*
1022 *Biophysical Research Communications*, *506*(4), 997–1003.
1023 https://doi.org/10.1016/j.bbrc.2018.10.190
1024 Malone, J. G., Jaeger, T., Manfredi, P., Dötsch, A., Blanka, A., Bos, R., Cornelis, G. R.,
1025 Häussler, S., & Jenal, U. (2012). The YfiBNR Signal Transduction Mechanism Reveals
1026 Novel Targets for the Evolution of Persistent Pseudomonas aeruginosa in Cystic

1027 Fibrosis Airways. *PLOS Pathogens*, *8*(6), e1002760.
1028 https://doi.org/10.1371/journal.ppat.1002760
1029 Malone, J. G., Jaeger, T., Spangler, C., Ritz, D., Spang, A., Arrieumerlou, C., Kaever, V.,
1030 Landmann, R., & Jenal, U. (2010). YfiBNR Mediates Cyclic di-GMP Dependent Small
1031 Colony Variant Formation and Persistence in Pseudomonas aeruginosa. *PLOS*
1032 *Pathogens*, *6*(3), e1000804. https://doi.org/10.1371/journal.ppat.1000804
1033 Malone, J. G., Williams, R., Christen, M., Jenal, U., Spiers, A. J., & Rainey, P. B. 2007. (2007).
1034 The structure–function relationship of WspR, a Pseudomonas fluorescens response
1035 regulator with a GGDEF output domain. *Microbiology*, *153*(4), 980–994.
1036 https://doi.org/10.1099/mic.0.2006/002824-0
1037 Manta, B., Boyd, D., & Berkmen, M. (2019). Disulfide Bond Formation in the Periplasm of
1038 Escherichia coli. *EcoSal Plus*, *8*(2). https://doi.org/10.1128/ecosalplus.ESP-0012-2018
1039 Martin, M., Hölscher, T., Dragoš, A., Cooper, V. S., & Kovács, Á. T. (2016). Laboratory
1040 Evolution of Microbial Interactions in Bacterial Biofilms. *Journal of Bacteriology*, *198*(19),
1041 2564–2571. https://doi.org/10.1128/jb.01018-15
1042 Marvig, R. L., Sommer, L. M., Molin, S., & Johansen, H. K. (2015). Convergent evolution and
1043 adaptation of Pseudomonas aeruginosa within patients with cystic fibrosis. *Nature*
1044 *Genetics*, *47*(1), 57–64. https://doi.org/10.1038/ng.3148
1045 McDonald, M. J., Gehrig, S. M., Meintjes, P. L., Zhang, X.-X., & Rainey, P. B. (2009). Adaptive
1046 Divergence in Experimental Populations of Pseudomonas fluorescens. IV. Genetic
1047 Constraints Guide Evolutionary Trajectories in a Parallel Adaptive Radiation. *Genetics*,
1048 *183*(3), 1041–1053. https://doi.org/10.1534/genetics.109.107110
1049 McFarland, A. G., Bertucci, H. K., Littman, E., Shen, J., Huttenhower, C., & Hartmann, E. M.
1050 (2021). Triclosan Tolerance Is Driven by a Conserved Mechanism in Diverse

Pseudomonas Species. *Applied and Environmental Microbiology*. https://doi.org/10.1128/AEM.02924-20

Mhatre, E., Snyder, D. J., Sileo, E., Turner, C. B., Buskirk, S. W., Fernandez, N. L., Neiditch, M. B., Waters, C. M., & Cooper, V. S. (2020). One gene, multiple ecological strategies: A biofilm regulator is a capacitor for sustainable diversity. *Proceedings of the National Academy of Sciences*, *117*(35), 21647–21657. https://doi.org/10.1073/pnas.2008540117

Nadell, C. D., Drescher, K., & Foster, K. R. (2016). Spatial structure, cooperation and competition in biofilms. *Nature Reviews Microbiology*, *14*(9), 589–600. https://doi.org/10.1038/nrmicro.2016.84

Oakley, J. L., Weiser, R., Powell, L. C., Forton, J., Mahenthiralingam, E., Rye, P. D., Hill, K. E., Thomas, D. W., & Pritchard, M. F. (2021). Phenotypic and Genotypic Adaptations in Pseudomonas aeruginosa Biofilms following Long-Term Exposure to an Alginate Oligomer Therapy. *mSphere*, *6*(1), 10.1128/msphere.01216-20. https://doi.org/10.1128/msphere.01216-20

O'Connor, J. R., Kuwada, N. J., Huangyutitham, V., Wiggins, P. A., & Harwood, C. S. (2012). Surface sensing and lateral subcellular localization of WspA, the receptor in a chemosensory-like system leading to c-di-GMP production. *Molecular Microbiology*, *86*(3), 720–729. https://doi.org/10.1111/mmi.12013

O'Neal, L., Baraquet, C., Suo, Z., Dreifus, J. E., Peng, Y., Raivio, T. L., Wozniak, D. J., Harwood, C. S., & Parsek, M. R. (2022). The Wsp system of Pseudomonas aeruginosa links surface sensing and cell envelope stress. *Proceedings of the National Academy of Sciences*, *119*(18), e2117633119. https://doi.org/10.1073/pnas.2117633119

O'Rourke, D., FitzGerald, C. E., Traverse, C. C., & Cooper, V. S. (2015). There and back again: Consequences of biofilm specialization under selection for dispersal. *Frontiers in Genetics*, *6*, 18. https://doi.org/10.3389/fgene.2015.00018

O'Toole, G. A., & Kolter, R. (1998). Initiation of biofilm formation in Pseudomonas fluorescens WCS365 proceeds via multiple, convergent signalling pathways: A genetic analysis. *Molecular Microbiology*, *28*(3), 449–461. https://doi.org/10.1046/j.1365-2958.1998.00797.x

Phippen, C. W., Mikolajek, H., Schlaefli, H. G., Keevil, C. W., Webb, J. S., & Tews, I. (2014). Formation and dimerization of the phosphodiesterase active site of the Pseudomonas aeruginosa MorA, a bi-functional c-di-GMP regulator. *FEBS Letters*, *588*(24), 4631–4636. https://doi.org/10.1016/j.febslet.2014.11.002

Poltak, S. R., & Cooper, V. S. (2011). Ecological succession in long-term experimentally evolved biofilms produces synergistic communities. *The ISME Journal*, *5*(3), 369–378. https://doi.org/10.1038/ismej.2010.136

Quigley, C. F., Zhao, Z., Cho, N., Matela, A., Siatkowski, C., Thiagarajan, S., & Cooper, V. (2025, January). *EvolvingSTEM: Exploring Authentic Research Experiences Effects on STEM Occupational Identity Development for Grades 6-12*. The Association for Science Teacher Education (ASTE) Meeting, Long Beach, CA.

Rainey, P. B., & Travisano, M. (1998). Adaptive radiation in a heterogeneous environment. *Nature*, *394*(6688), 69–72. https://doi.org/10.1038/27900

Røder, H. L., Sørensen, S. J., & Burmølle, M. (2016). Studying Bacterial Multispecies Biofilms: Where to Start? *Trends in Microbiology*, *24*(6), 503–513. https://doi.org/10.1016/j.tim.2016.02.019

1096 Rybtke, M. T., Borlee, B. R., Murakami, K., Irie, Y., Hentzer, M., Nielsen, T. E., Givskov, M.,
1097 Parsek, M. R., & Tolker-Nielsen, T. (2012). Fluorescence-based reporter for gauging
1098 cyclic di-GMP levels in Pseudomonas aeruginosa. *Applied and Environmental*
1099 *Microbiology*, *78*(15), 5060–5069. https://doi.org/10.1128/AEM.00414-12
1100 Santos-Lopez, A., Marshall, C. W., Scribner, M. R., Snyder, D. J., & Cooper, V. S. (2019).
1101 Evolutionary pathways to antibiotic resistance are dependent upon environmental
1102 structure and bacterial lifestyle. *eLife*, *8*, e47612. https://doi.org/10.7554/eLife.47612
1103 Schindelin, J., Arganda-Carreras, I., Frise, E., Kaynig, V., Longair, M., Pietzsch, T., Preibisch,
1104 S., Rueden, C., Saalfeld, S., Schmid, B., Tinevez, J.-Y., White, D. J., Hartenstein, V.,
1105 Eliceiri, K., Tomancak, P., & Cardona, A. (2012). Fiji: An open-source platform for
1106 biological-image analysis. *Nature Methods*, *9*(7), 676–682.
1107 https://doi.org/10.1038/nmeth.2019
1108 Schweizer, H. P. (2001). Triclosan: A widely used biocide and its link to antibiotics. *FEMS*
1109 *Microbiology Letters*, *202*(1), 1–7. https://doi.org/10.1111/j.1574-6968.2001.tb10772.x
1110 Scribner, M. R., Santos-Lopez, A., Marshall, C. W., Deitrick, C., & Cooper, V. S. (2020). Parallel
1111 Evolution of Tobramycin Resistance across Species and Environments. *mBio*, *11*(3),
1112 e00932-20. https://doi.org/10.1128/mBio.00932-20
1113 Smith, E. E., Buckley, D. G., Wu, Z., Saenphimmachak, C., Hoffman, L. R., D'Argenio, D. A.,
1114 Miller, S. I., Ramsey, B. W., Speert, D. P., Moskowitz, S. M., Burns, J. L., Kaul, R., &
1115 Olson, M. V. (2006). Genetic adaptation by Pseudomonas aeruginosa to the airways of
1116 cystic fibrosis patients. *Proceedings of the National Academy of Sciences*, *103*(22),
1117 8487–8492. https://doi.org/10.1073/pnas.0602138103
1118 Spiers, A. J., Bohannon, J., Gehrig, S. M., & Rainey, P. B. (2003). Biofilm formation at the air–
1119 liquid interface by the Pseudomonas fluorescens SBW25 wrinkly spreader requires an

acetylated form of cellulose. *Molecular Microbiology*, *50*(1), 15–27. https://doi.org/10.1046/j.1365-2958.2003.03670.x

Spiers, A. J., Kahn, S. G., Bohannon, J., Travisano, M., & Rainey, P. B. (2002). Adaptive Divergence in Experimental Populations of Pseudomonas fluorescens. I. Genetic and Phenotypic Bases of Wrinkly Spreader Fitness. *Genetics*, *161*(1), 33–46. https://doi.org/10.1093/genetics/161.1.33

States, N. L. (2013). *Next Generation Science Standards: For States, By States*. National Academies Press.

Stewart, P. S., & Franklin, M. J. (2008). Physiological heterogeneity in biofilms. *Nature Reviews Microbiology*, *6*(3), 199–210. https://doi.org/10.1038/nrmicro1838

Trampari, E., Holden, E. R., Wickham, G. J., Ravi, A., Martins, L. de O., Savva, G. M., & Webber, M. A. (2021). Exposure of Salmonella biofilms to antibiotic concentrations rapidly selects resistance with collateral tradeoffs. *Npj Biofilms and Microbiomes*, *7*(1), 1–13. https://doi.org/10.1038/s41522-020-00178-0

Traverse, C. C., Mayo-Smith, L. M., Poltak, S. R., & Cooper, V. S. (2013). Tangled bank of experimentally evolved Burkholderia biofilms reflects selection during chronic infections. *Proceedings of the National Academy of Sciences*, *110*(3), E250–E259. https://doi.org/10.1073/pnas.1207025110

Trubenová, B., Roizman, D., Moter, A., Rolff, J., & Regoes, R. R. (2022). Population genetics, biofilm recalcitrance, and antibiotic resistance evolution. *Trends in Microbiology*, *30*(9), 841–852. https://doi.org/10.1016/j.tim.2022.02.005

Turner, C. B., Marshall, C. W., & Cooper, V. S. (2018). Parallel genetic adaptation across environments differing in mode of growth or resource availability. *Evolution Letters*, *2*(4), 355–367. https://doi.org/10.1002/evl3.75

1144 Wei, Q., Leclercq, S., Bhasme, P., Xu, A., Zhu, B., Zhang, Y., Zhang, M., Wang, S., & Ma, L. Z.
1145 (2019). Diguanylate Cyclases and Phosphodiesterases Required for Basal-Level c-di-
1146 GMP in Pseudomonas aeruginosa as Revealed by Systematic Phylogenetic and
1147 Transcriptomic Analyses. *Applied and Environmental Microbiology*, *85*(21), e01194-19.
1148 https://doi.org/10.1128/AEM.01194-19
1149 Xu, A., Wang, D., Wang, Y., Zhang, L., Xie, Z., Cui, Y., Bhamse, P., Yu, H., Zhang, X.-X., Li, D.,
1150 & Ma, L. Z. (2021). Mutations in surface-sensing receptor WspA lock the Wsp signal
1151 transduction system into a constitutively active state. *Environmental Microbiology*,
1152 *n/a*(n/a). https://doi.org/10.1111/1462-2920.15763
1153 Xu, M., Yang, X., Yang, X.-A., Zhou, L., Liu, T.-Z., Fan, Z., & Jiang, T. (2016). Structural insights
1154 into the regulatory mechanism of the Pseudomonas aeruginosa YfiBNR system. *Protein*
1155 *& Cell*, *7*(6), 403–416. https://doi.org/10.1007/s13238-016-0264-7
1156 Yang, X., Yang, X., Xu, M., Zhou, L., Fan, Z., & Jiang, T. (2015). Crystal structures of YfiR from
1157 Pseudomonas aeruginosa in two redox states. *Biochemical and Biophysical Research*
1158 *Communications*, *461*(1), 14–20. https://doi.org/10.1016/j.bbrc.2015.03.160
1159 Yu, L., Cao, Q., Chen, W., Yang, N., Yang, C.-G., Ji, Q., Wu, M., Bae, T., & Lan, L. (2022). A
1160 novel copper-sensing two-component system for inducing Dsb gene expression in
1161 bacteria. *Science Bulletin*, *67*(2), 198–212. https://doi.org/10.1016/j.scib.2021.03.003
1162 Zhao, K., Tseng, B. S., Beckerman, B., Jin, F., Gibiansky, M. L., Harrison, J. J., Luijten, E.,
1163 Parsek, M. R., & Wong, G. C. L. (2013). Psl trails guide exploration and microcolony
1164 formation in Pseudomonas aeruginosa biofilms. *Nature*, *497*(7449), 388–391.
1165 https://doi.org/10.1038/nature12155
1166